Article

SOURCE DATA | TRANSPARENT PROCESS | OPEN ACCESS

THE EMBO JOURNAL

TBK1 phosphorylates mutant Huntingtin and suppresses its aggregation and toxicity in Huntington's disease models

Ramanath Narayana Hegde[1], Anass Chiki[1], Lara Petricca[2], Paola Martufi[2], Nicolas Arbez[3], Laurent Mouchiroud[4], Johan Auwerx[4], Christian Landles[5], Gillian P Bates[5], Malvindar K Singh-Bains[6], Mike Dragunow[7], Maurice A Curtis[6], Richard LM Faull[6], Christopher A Ross[3], Andrea Caricasole[2] & Hilal A Lashuel[1,*]

Abstract

Phosphorylation of the N-terminal domain of the huntingtin (HTT) protein has emerged as an important regulator of its localization, structure, aggregation, clearance and toxicity. However, validation of the effect of *bona fide* phosphorylation *in vivo* and assessing the therapeutic potential of targeting phosphorylation for the treatment of Huntington's disease (HD) require the identification of the enzymes that regulate HTT phosphorylation. Herein, we report the discovery and validation of a kinase, TANK-binding kinase 1 (TBK1), that efficiently phosphorylates full-length and N-terminal HTT fragments *in vitro* (at S13/S16), in cells (at S13) and *in vivo*. TBK1 expression in HD models (cells, primary neurons, and *Caenorhabditis elegans*) increases mutant HTT exon 1 phosphorylation and reduces its aggregation and cytotoxicity. We demonstrate that the TBK1-mediated neuroprotective effects are due to phosphorylation-dependent inhibition of mutant HTT exon 1 aggregation and an increase in autophagic clearance of mutant HTT. These findings suggest that upregulation and/or activation of TBK1 represents a viable strategy for the treatment of HD by simultaneously lowering mutant HTT levels and blocking its aggregation.

Keywords autophagy; huntingtin phosphorylation; Huntington's disease; reducing aggregation; TBK1

Subject Categories Molecular Biology of Disease; Neuroscience

DOI 10.15252/embj.2020104671 | Received 11 February 2020 | Revised 9 June 2020 | Accepted 16 June 2020

The EMBO Journal (2020) e104671

Introduction

Huntington's disease (HD) is an autosomal dominant, progressive neurodegenerative disease caused by a CAG triplet repeat expansion (> 35) in the *huntingtin* gene. This translates into a polyglutamine (polyQ) repeat immediately following the first 17 amino acids (N17) in the Huntingtin protein (HTT). PolyQ repeats in the disease range (> 36, hereafter denoted as mutant HTT) render HTT more susceptible to misfolding, thus leading to the formation of HTT aggregates in cells and neurons (Scherzinger *et al*, 1999; Caron *et al*, 2013; Cui *et al*, 2014; Fodale *et al*, 2014; Daldin *et al*, 2017). Increasing evidence from human studies has shown that expansion of the polyQ repeat is the causative mutation of HD but not the only contributor to disease onset, duration, and severity (Wexler *et al*, 2004; Andresen *et al*, 2007; Lee *et al*, 2019). This suggests that other factors may play important roles in modifying the course of the disease and potentially the patient response to therapies.

Post-translational modifications (PTMs), particularly within the N17 of the HTT protein, have emerged as key regulators of HTT stability, clearance, localization, proteolysis, aggregation, and toxicity in different models of HD (Ehrnhoefer *et al*, 2011; Saudou & Humbert, 2016), including mouse HD models (Gu *et al*, 2009). These studies were largely based on the mutation of PTM-targeted residues to mimic or abolish the presence of relevant PTMs. Among all the putative PTMs that have been identified in the HTT protein, phosphorylation at the N-terminal serine residues S13 and S16 is the most studied for the following reasons: (i) It occurs on several residues in close proximity to the polyQ domain and within the N17

1 Laboratory of Molecular and Chemical Biology of Neurodegeneration, Brain Mind Institute, École Polytechnique Fédérale de Lausanne (EPFL), Lausanne, Switzerland
2 Department of Neuroscience, IRBM Science Park, Rome, Italy
3 Division of Neurobiology, Department of Psychiatry and Departments of Neurology, Neuroscience and Pharmacology, Johns Hopkins University School of Medicine, Baltimore, MD, USA
4 Laboratory of Integrative and Systems Physiology, École Polytechnique Fédérale de Lausanne (EPFL), Lausanne, Switzerland
5 Huntington's Disease Centre, Department of Neurodegenerative Disease and UK Dementia Research Institute at UCL, Queen Square Institute of Neurology, University College London, London, UK
6 Centre for Brain Research, Department of Anatomy and Medical Imaging, University of Auckland, Auckland, New Zealand
7 Centre for Brain Research, Department of Pharmacology and Clinical Pharmacology, University of Auckland, Auckland, New Zealand
*Corresponding author. Tel: +41 21 693 96 91; E-mail: hilal.lashuel@epfl.ch

domain, which has been shown to play important roles in regulating HTT structure, aggregation, and subcellular localization (Rockabrand *et al*, 2007; Gu *et al*, 2009; Thompson *et al*, 2009); (ii) mimicking phosphorylation at these residues in the context of the full-length mutant HTT protein (S13D/S16D) in mice was sufficient to ameliorate HD phenotypes, including motor and psychiatric-like behavioral deficits, mutant HTT aggregation, and selective neurodegeneration (Gu *et al*, 2009); and (iii) the levels of phosphorylation at T3 and S13/S16 are reduced in HD models (Thompson *et al*, 2009; Atwal *et al*, 2011; Cariulo *et al*, 2019). These observations suggest that targeting HTT PTMs at N17 represents a viable strategy for developing novel disease-modifying therapies for HD. The first step towards assessing the therapeutic potential of targeting N17 PTMs for the treatment of HD is the identification of the enzymes that regulate these PTMs. This is important because increasing evidence shows that phosphorylation-mimicking mutations (e.g., serine (S) or threonine (T) to aspartate (D) or glutamate (E)) used to investigate the effects of protein phosphorylation may not fully phenocopy the effects of the *bona fide* modifications (Szczepanowska *et al*, 1998; Paleologou *et al*, 2008; Dephoure *et al*, 2013; Chiki *et al*, 2017; Deguire *et al*, 2018) and do not faithfully reproduce the dynamic nature of phosphorylation.

We and others have shown that phosphorylation or introduction of phosphomimicking mutations at S13 and/or S16 inhibit the aggregation of mutant HTTex1 or HTTex1 model peptides (Gu *et al*, 2009; Mishra *et al*, 2012; Deguire *et al*, 2018) and increases HTTex1 conformational flexibility *in vitro* (Daldin *et al*, 2017). A direct comparison of the effect of phosphomimetics and *bona fide* phosphorylation at these sites showed that the phosphomimetic (S13D/S16D) only partially reproduced the effect of phosphorylation on HTTex 1 aggregation *in vitro* and did not reproduce the effect of single and double phosphorylation at these residues on the helical conformation of N17 peptides (Deguire *et al*, 2018). Moreover, a recent study using a *Drosophila* model of HD expressing HTTex1 97Q showed that both S13D and S16D increase aggregation (Branco-Santos *et al*, 2017), in contrast to observations in mammalian cell models of HD showing that the N-terminal fragments of HTT 1-171 142Q, HTTex1 97Q, or HTTex1 82Q with S13D and S16D with S13D and S16D exhibit decreased aggregation and toxicity (Atwal *et al*, 2011; Arbez *et al*, 2017; Branco-Santos *et al*, 2017). These findings show that PTMs, such as single or double phosphorylation, are sufficient to modify mutant HTT levels, aggregation, and toxicity, but also emphasize the importance of identifying the natural kinases involved in regulating HTT phosphorylation to assess the biological relevance and therapeutic potential of *bona fide* phosphorylation at these residues.

In the current study, we sought to identify the natural kinases that efficiently phosphorylate HTT at S13 and S16, with the aim of using these kinases to assess the therapeutic potential of phosphorylation at these residues by investigating its effect on mutant HTT aggregation, clearance, and toxicity in cellular and animal models of HD. Using an *in vitro* screen of ~300 serine and threonine kinases, we identified TANK-binding kinase 1 (TBK1) as one of the most promising candidate kinases. In an *in vitro* phosphorylation assays, TBK1 induced site-specific and quantitative phosphorylation of both wild-type and mutant HTT at both residues S13 and S16. TBK1 is known to regulate the innate immune response and belongs to the IκB kinase family that includes other kinases such as IKKβ. Previously, IKKβ was shown to phosphorylate HTT at these residues (Thompson *et al*, 2009) as well as at residue T3 (Bustamante *et al*, 2015), and was recently shown to increase HTT S13 phosphorylation in HD and wild-type mice (Ochaba *et al*, 2019). In this work, the specificity and efficiency of TBK1 for phosphorylating full-length and N-terminal fragments of HTT (HTTex1, HTTN548, HTT-fl) were validated *in vitro* using recombinant proteins, in mammalian cells, in primary neuronal culture and *in vivo* via overexpression of the wild-type and kinase-dead variant of TBK1. Next, we assessed the effect of TBK1-mediated phosphorylation on HTT levels, subcellular localization, aggregation, and toxicity in cellular, neuronal, and *Caenorhabditis elegans* (*C. elegans*) models of HD. In all these model systems, we observed that TBK1 phosphorylated the HTT protein at S13, decreased its levels, inhibited its aggregation, and suppressed its toxicity. Furthermore, mechanistic studies showed that these effects were mediated by both TBK1-dependent phosphorylation of HTT, which stabilized the protein and blocked its aggregation, and TBK1-mediated increased autophagic flux, which also promoted the clearance of HTT, leading to a decrease in HTT aggregation. Together, our results show that increasing phosphorylation at S13 and/or TBK1 activation or upregulation represent viable therapeutic strategies for the treatment of HD.

Results

Identification of TBK1 as a kinase that efficiently phosphorylates HTT at S13 in cellular models of HD

To discover kinases responsible for phosphorylating HTT at S13 and S16, we used a commercial *in vitro* kinase screening assay (Kinexus *in vitro* kinase and phospho-peptide testing (IKPT) services), which includes ~300 kinases (Binukumar *et al*, 2016). The screen was carried out using two HTT substrates: a peptide that comprises the first 17 N-terminal residues of HTT (N17), and the first exon of the HTT protein (HTTex1) (Fig 1A–C). After an extensive *in vitro* validation using the top kinase hits from the screen, which included monitoring of the extent of phosphorylation using mass spectrometry as well as by the use of previously validated phospho-antibodies against T3 (pT3), S13 (pS13), and S16 (pS16) (Bustamante *et al*, 2015; Deguire *et al*, 2018; Cariulo *et al*, 2019), TBK1 was identified as the only kinase that selectively and robustly phosphorylated HTTex1 *in vitro* at S13 and S16 (Figs 1C and EV1A–E). Additionally, TBK1-mediated phosphorylation of the longer N-terminal fragments resulted predominantly in diphosphorylation at both S13 and S16, along with a small amount of tri-phosphorylated and traces of tetra-phosphorylated species for some of the longer N-terminal HTT fragments (Fig EV1A and B). For these substrates and HTTex1, a signal was observed for only the pS13 and pS16 antibodies, demonstrating that TBK1 did not phosphorylate HTTex1 at T3 (Fig EV1A and B lower panel). Consistent with these data, we did not observe any phosphorylation of a HTTex1 mutant in which both residues were mutated to aspartate (S13D/S16D), even after extended periods of incubation with TBK1 (Fig EV1C–E).

The TBK1 family kinase IKKβ was previously reported to phosphorylate HTT at S13/S16 (Thompson *et al*, 2009). Therefore, we sought to compare the efficiency of TBK1- and IKKβ-mediated phosphorylation of HTTex1. To this end, we compared the kinetics and

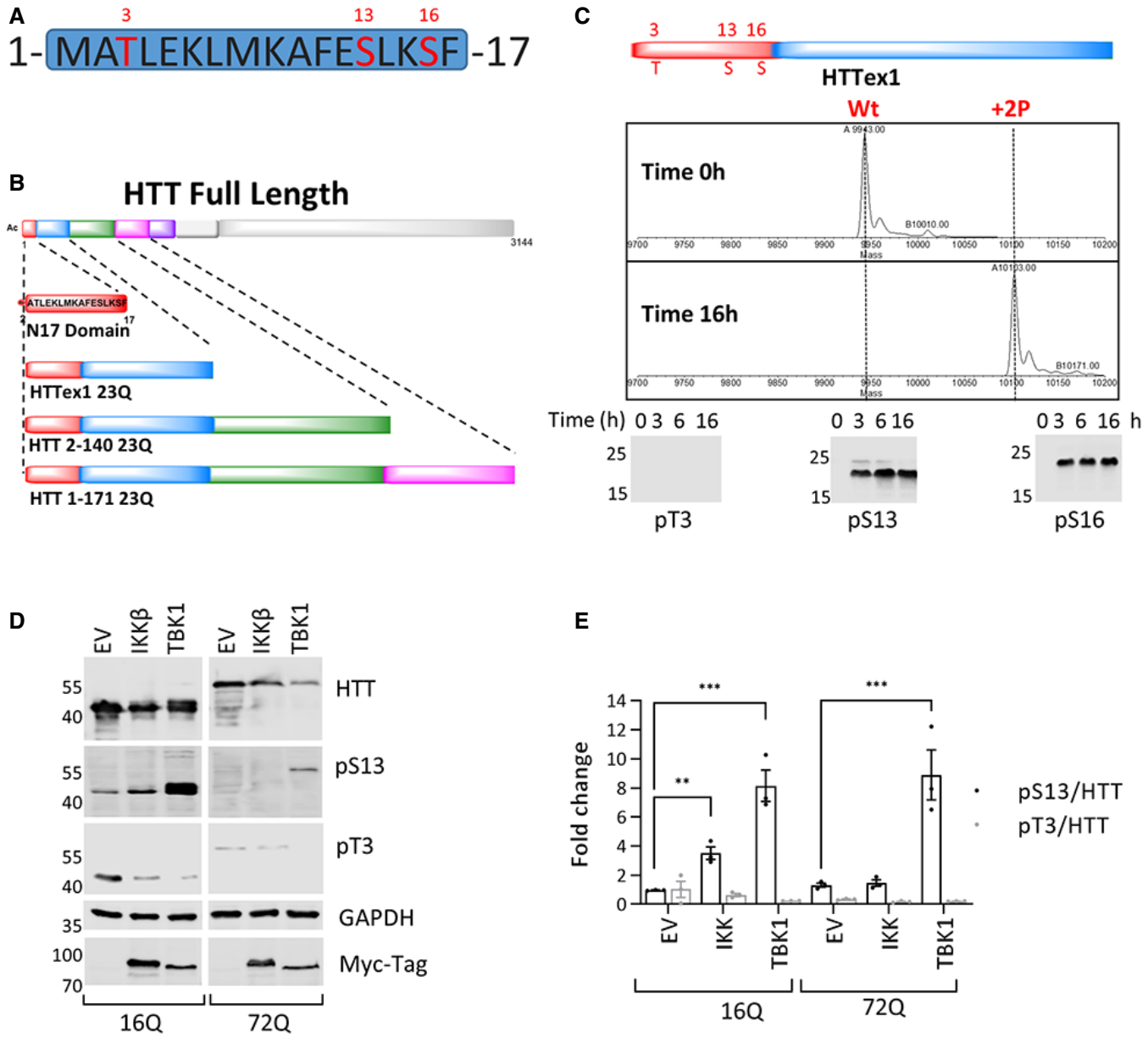

Figure 1. Identification of TBK1 as a kinase that efficiently phosphorylates HTT at S13 in cellular models of HD.

A Potential phosphorylation sites in the HTT N17 domain (T3, S13, and S16).

B List of all the different substrates used for the *in vitro* kinase validation: Nt17, HTTex1, and HTT longer fragments.

C Mass spectra of recombinant HTTex1 23Q after 16 h of co-incubation with TBK1 showing complete phosphorylation of S13 and S16. The lower panel is a representative Western blot of the same phosphorylation reaction (upper panel) using anti-pT3 (CHDI-90001528-1), pS13 HTT (CHDI-90001039-1), and pS16 (ZCH11020 generated in house) antibodies (ab) after the indicated phosphorylation reaction times.

D Representative Western blot of HTT (ab-MAB5492), HTT pS13 (ab-CHDI-90001039-1), and HTT pT3 (ab-CHDI-90001528-1) upon coexpression of HTTex1 16Q and 72Q eGFP with the indicated kinases for 48 h in HEK293 cells.

E Quantification of the fold changes in the HTT pS13 and pT3 ratios to total HTT compared to empty vector (EV) control upon coexpression of the indicated kinase from the experiments like in D.

Data information: Graph reports mean ± SEM, $n = 3$. Significance was assessed using 2-tailed Student's *t*-test, < 0.001***, 0.001 to 0.01**.
Source data are available online for this figure.

efficiency of HTTex1 phosphorylation by these two kinases. As shown in Appendix Fig S1A–D, we observed significantly faster phosphorylation by TBK1 than by IKKβ at both S13 and S16 residues. IKKβ seemed to require a longer time to phosphorylate HTT. After 6 h, TBK1 resulted in almost complete diphosphorylation, whereas IKKβ showed predominantly mono-phosphorylated HTT even after 16 h, with a significant amount of non-phosphorylated HTT remaining (Appendix Fig S1B and D). This observed difference

may also be due to the difference in activity of TBK1 and IKKβ as efficient activity of the later may need IKK complex subunits IKKα and IKKγ. Collectively, these findings demonstrate that TBK1 efficiently and site-specifically phosphorylates recombinant HTT at S13 and S16 *in vitro,* suggesting that it could be one of the natural kinases that may regulate HTT phosphorylation and cellular properties *in vivo*.

Next, to determine whether TBK1 phosphorylates the N-terminal domain of HTT in cells, we assessed the level of phosphorylation at S13 upon coexpression of wild-type (16Q) or mutant (72Q) HTTex1 with TBK1 in HEK293 cells by Western blot (WB) using the phospho-antibodies against T3 (pT3) and S13 (pS13). We observed that TBK1 coexpression for 48 h led to a strong ~5- to 10-fold increase in phosphorylation at S13 (Fig 1D and E) compared to empty vector (EV) control. Before this study, IKKβ was reported to phosphorylate HTT at S13/S16 with a preference for HTT containing unexpanded polyQ repeats (Thompson *et al*, 2009). Therefore, we sought to compare the phosphorylation efficiency of TBK1 and IKKβ on mutant and wild-type HTTex1. As shown in Fig 1D and E, IKKβ indeed phosphorylated HTTex1 16Q more efficiently than 72Q, but the phosphorylation levels were much lower than the levels achieved upon coexpression with TBK1, consistent with our *in vitro* data (Appendix Fig S1A and D). However, this comparison may not be accurate as the activity of IKKβ could be influenced by IKKα and IKKγ, which may work together within the IKK complex.

In our *in vitro* assay, we observed that TBK1 phosphorylated HTT at both S13 and S16, but due to the lack of a specific antibody that recognizes phosphorylation at S16 in cell lysates, we could not directly evaluate whether TBK1 phosphorylated S16 in cellular models by WB. To confirm the sites of phosphorylation in cells, we performed MS/MS analysis of HTTex1 immunoprecipitated from TBK1 and TBK1 KD coexpressing wild-type 16Q HTTex1 HEK293 cells. While we detected the phosphorylation at S13, we did not observe any phosphorylation at S16 on HTT under these conditions (Fig EV2A and B). These results suggest that TBK1 phosphorylates HTT at S13 but not at S16 in cells, whereas both sites are efficiently phosphorylated *in vitro* (Fig 1C).

Next, we asked whether the kinase activity of TBK1 was required for the phosphorylation of HTT. To answer this question, we compared the level of phosphorylation at S13 upon coexpression of HTTex1 16Q or 72Q with wild-type TBK1 or a TBK1 kinase-dead (TBK1 KD) mutant (K38A; Richter *et al*, 2016). While WT TBK1 increased S13 phosphorylation, no significant increase in phosphorylation was detected upon expression of TBK1 KD (Fig 2A and B). This confirms that HTT S13 phosphorylation is dependent on the catalytic activity of TBK1. Next, we sought to verify the site specificity of TBK1 phosphorylation of HTT in cells. To this end, we coexpressed HTT with alanine mutations at residue 3 (T3A) or residues 13/16 (S13A/S16A) with TBK1 or TBK1 KD. We observed that TBK1 did not phosphorylate HTTex1 S13A/S16A but phosphorylated S13 on HTTex1 T3A (Fig 2A and B), confirming that TBK1 specifically phosphorylates S13 on HTTex1. Interestingly, we observed residual phosphorylation at S13 in TBK1 KD, which could be due to other endogenous kinases, including but not limited to IKKβ. In contrast to previous reports (Thompson *et al*, 2009) and our observations for IKKβ in this study, TBK1 phosphorylated both wild-type and mutant HTTex1 with the same efficiency (Figs 1D and E and 2A and B). These findings suggest that the polyQ expansion does not significantly influence TBK1-dependent phosphorylation of S13.

Having established that TBK1 phosphorylated HTTex1 and other fragments in different cellular models, we sought to determine whether TBK1 interacts directly with its HTT substrates. To this end, we coexpressed TBK1 or TBK1 KD with wild-type HTTex1 16Q or HTTex1 72Q or bearing the S13A/S16A mutation for 48 h in HEK293 cells and immunoprecipitated HTT. We observed that TBK1 specifically co-immunoprecipitated with HTTex1 irrespective of the presence or absence of the S13A/S16A mutation (Fig EV2C and D). These results suggest that both wild-type and mutant HTTex1 may interact with TBK1 in cells and that the phosphorylation-blocking mutations at S13 and S16 do not influence the HTT-TBK1 interaction.

Under physiological conditions, HTT exists as a mixture of different N-terminal fragments and full-length HTT (Mende-Mueller *et al*, 2001). Therefore, we sought to examine whether TBK1 could phosphorylate longer N-terminal fragments and full-length HTT proteins. We coexpressed either the mutant HTTN548 (55Q) fragment or a full-length mutant HTT (HTT-fl 48Q) with TBK1 or TBK1 KD in HEK293T cells and analyzed S13 phosphorylation by WB using an HTT pS13 antibody and using a new, sensitive Singulex assay (Cariulo *et al*, 2019). We observed by WB that TBK1 phosphorylated both the HTTN548 55Q fragment (Fig 2C) and HTT-fl 48Q at S13 (Fig 2E). Quantitative Singulex immunoassay analysis of cell lysates showed that TBK1 coexpression led to approximately 60- and 20-fold increases in phosphorylation at S13 of HTTN548 55Q (Fig 2D) and HTT-fl 48Q (Fig 2F), respectively. As expected, we did not observe any significant increase in phosphorylation upon coexpression of TBK1 or TBK1 KD with HTT-fl 48Q bearing the S13A and S16A mutations (Fig 2F). We further assessed whether TBK1 could phosphorylate endogenous HTT in neurons. We overexpressed TBK1 or TBK1 KD using lentivirus-mediated transduction in rat primary striatal neuronal cultures. Striatal medium spiny neurons are most affected in HD (Ehrlich, 2012), and striatal cells have been used as a model for HD studies (Trettel *et al*, 2000). We immunoprecipitated endogenous HTT from these striatal culture lysates using the HTT antibody D7F7, followed by immunoblotting with an anti-pS13 antibody. We observed an increased level of HTT pS13, but not pT3 upon TBK1 expression. This confirmed that TBK1 phosphorylated endogenous HTT at S13 (Fig 2G and H). Next, to investigate whether TBK1 is one of the endogenous enzymes involved in regulating the levels of endogenous phosphorylation of HTT at S13, we assessed S13 phosphorylation after a genetic knockdown or pharmacological inhibition of TBK1 in primary neurons. We treated rat primary striatal neurons with TBK1 kinase inhibitors for 48 h or with siRNA for 72 h and assessed the effects on HTT and HTT pS13 levels using specific antibodies. As shown in Figure EV2E and F TBK1 knockdown did not lead to a significant change in HTT pS13 levels, but increased endogenous HTT levels by approximately 1.5- to 2-fold. We observed no change in pS13 levels but there was a trend toward an increase in endogenous HTT levels in the inhibitor-treated striatal neuronal cells (Fig EV2G and H). While these results clearly demonstrate that TBK1 is involved in regulating the turnover of endogenous HTT, no significant change in HTT pS13 levels caused by either inhibitor treatment or siRNA treatment was observed. This might be due to residual TBK1 kinase activity that could phosphorylate endogenous HTT. Alternatively, it is also

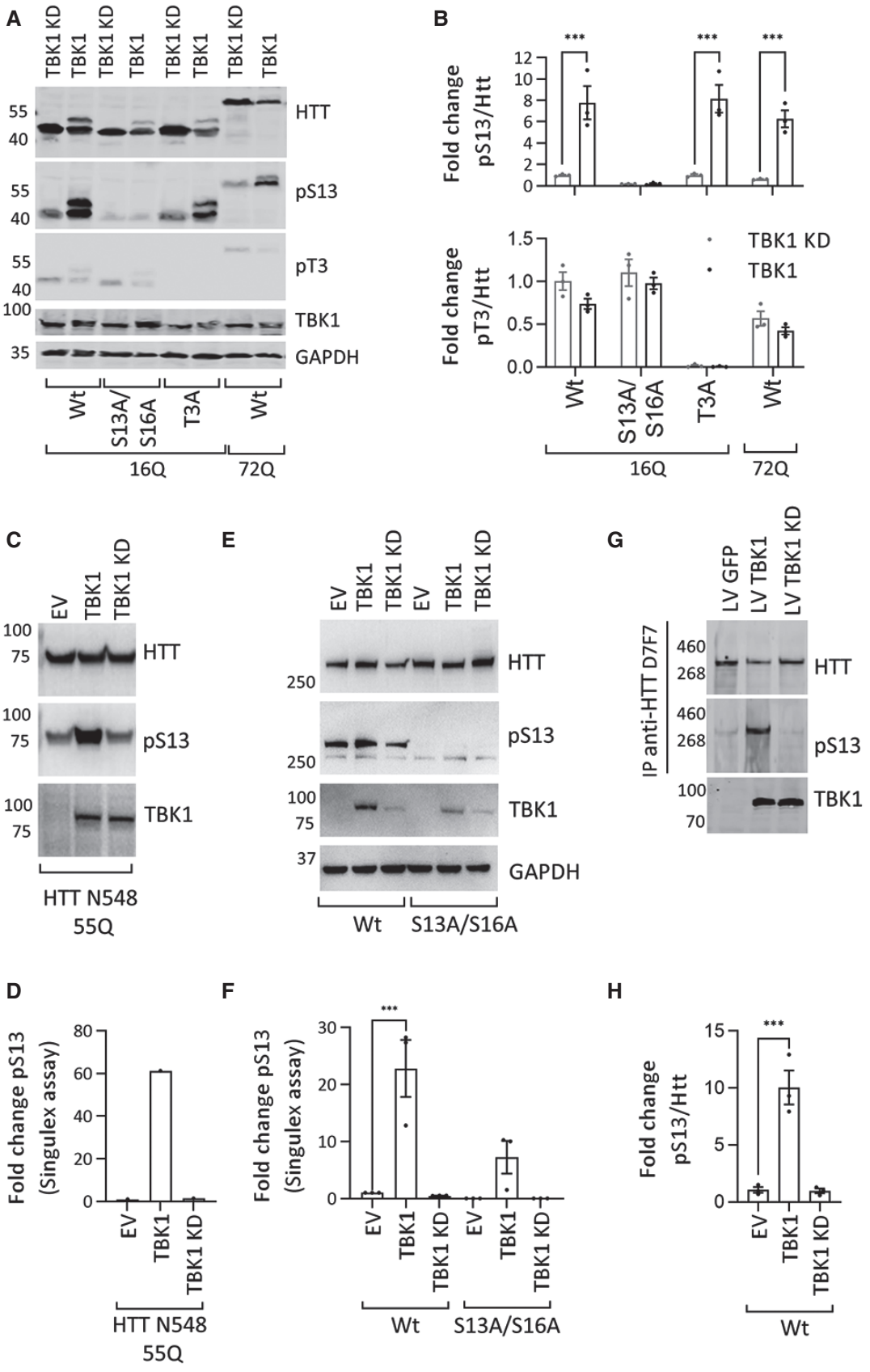
A
TBK1 KD
TBK1
HTT
pS13
pT3
TBK1
GAPDH
Wt
S13A/S16A
T3A
16Q
72Q
B
Fold change pS13/Htt
Fold change pT3/Htt
TBK1 KD
TBK1
C
EV
HTT N548 55Q
D
Fold change pS13 (Singulex assay)
E
Wt
S13A/S16A
F
G
LV GFP
LV TBK1
LV TBK1 KD
IP anti-HTT D7F7
H

Figure 2.

Figure 2. TBK1 phosphorylates HTT in cellular models.

A Representative Western blot of HTT (ab-MAB5492), HTT pS13 (ab-CHDI-90001039-1), and HTT pT3 (ab-CHDI-90001528-1) upon coexpression of HTTex1 16Q eGFP mutants with S to A substitutions at T3 or S13/S16 or HTTex1 72Q eGFP with TBK1 or TBK1 kinase-dead (KD) for 48 h in HEK293 cells (the additional high molecular weight HTTex1 and HTT pS13 band is possibly due to the co-occurrence of phosphorylation at both S13 and T3).

B Quantification of the fold changes in the HTT pS13 (upper panel) and pT3 (lower panel) ratio to total HTT compared to those of the kinase-dead mutant from the experiments like in A (n = 3).

C Representative Western blot of HTT (ab-MAB2166) and HTT pS13 (ab-CHDI-90001039-1) upon coexpression of HTT N543 55Q with the indicated kinase for 24 h in HEK293T cells.

D Quantification of HTT pS13 using the Singulex assay (using ab-MW1 as capture and CHDI-90001039 or 2B7 as detection antibodies for pS13 or total HTT) upon coexpression of HTT N543 55Q with the indicated kinase for 24 h in HEK293T cells from the experiment in C (representative of 3 repeats).

E Representative Western blot of HTT (ab-MAB2166) and HTT pS13 (ab-CHDI-90001039-1) upon coexpression of HTT-fl 48Q or HTT-fl 48Q S13A/S16A with the indicated kinase for 24 h in HEK293T cells.

F Quantification of HTT pS13 using the Singulex assay (using ab-MW1 as capture and CHDI-90001039 or 2B7 as detection antibodies for pS13 or total HTT) upon coexpression of HTT-fl 48Q or HTT-fl 48Q S13A/S16A with the indicated kinase for 24 h in HEK293T cells from the experiments like in E (n = 3).

G Representative Western blot of immunoprecipitated (IP) HTT (ab-MAB2166) and HTT pS13 (ab-CHDI-90001039-1) after lentivirus (LV)-mediated overexpression of TBK1 or TBK1 KD for 72 h in rat primary striatal neuronal cells.

H Quantification of the fold changes in the HTT pS13 ratio to total HTT compared to those of the kinase-dead mutant from the experiments like in G (n = 3).

Data information: Graphs report mean ± SEM. Significance was assessed using 2-tailed Student's t-test, < 0.001***.
Source data are available online for this figure.

possible that other kinases like IKKβ may phosphorylate HTT at S13 (Ochaba *et al*, 2019).

To clarify whether endogenous TBK1 phosphorylated HTT at S13 in the mammalian brain, we used a mouse model of *Tbk1*$^{-/-}$ on the *Tnf-α*$^{-/-}$ background (Hemmi *et al*, 2004). We dissected the cortices of P0 mouse pups from the *Tbk1*$^{+/+}$, *Tnf-α*$^{+/+}$ and *Tbk1*$^{-/-}$, *Tnf-α*$^{-/-}$ strains, lysed the tissues, and subjected the total protein extract to WB analysis to determine HTT and HTT pS13 levels. This double knockout model was previously used to investigate the function of TBK1 (Hemmi *et al*, 2004) because *Tbk1* knockout was embryonic lethal (Perry *et al*, 2004). Consistent with the knockdown and inhibitor experiments, we observed no change in pS13 HTT levels but there was an increase in the total HTT level (Fig EV2I and J). These observations may be explained by compensatory mechanisms involving other kinases, or homeostatic mechanisms involving downregulation of relevant phosphatases. However, the increased levels of HTT upon silencing or inhibition of TBK1 indicated an S13 phosphorylation independent role of TBK1 in HTT clearance. Moreover, we observed residual phosphorylation at S13 on HTT in our coexpression experiments which could also be due to IKKβ (Ochaba *et al*, 2019) or other kinases. These data collectively indicate that TBK1 regulates HTT levels, but there may be other kinases involved in the regulation of HTT phosphorylation at S13.

TBK1 overexpression affects HTT subcellular localization and reduces its aggregation and cytotoxicity

It has been reported that the first 17 amino acids of HTT have multiple roles in regulating the cellular properties of HTT, including its subcellular localization (Steffan *et al*, 2004; Atwal *et al*, 2007; Rockabrand *et al*, 2007). The HTT N17 domain was shown to contain a translocated promoter region (TPR)-dependent nuclear export signal (Steffan *et al*, 2004; Benn *et al*, 2005; Cornett *et al*, 2005; Atwal *et al*, 2007; Rockabrand *et al*, 2007; Maiuri *et al*, 2013). Mimicking phosphorylation at S13 and S16 (S13D/S16D) increased the localization of the HTT N17 peptide, HTTex1, or longer N-terminal HTT fragments to the nucleus (Thompson *et al*, 2009; Atwal *et al*, 2011; Havel *et al*, 2011; Zheng *et al*, 2013; Arbez *et al*, 2017). Moreover, we recently reported that single or double phosphorylation at S13 and/or S16 significantly enhanced the targeting of mutant HTTex1 fibrils to the nuclear compartment (Deguire *et al*, 2018). As TBK1 increased S13 phosphorylation, we hypothesized that this could also increase the nuclear localization of HTT. To test this hypothesis, we coexpressed wild-type or mutant HTTex1 and TBK1 or TBK1 KD in HEK293 cells and then comparatively assessed the levels of nuclear and cytosolic HTT by immunocytochemistry (ICC). We observed increased nuclear intensity of wild-type or mutant HTTex1 eGFP upon TBK1 coexpression (Fig EV3A and B). We also assessed the levels of HTT proteins biochemically in purified nuclear and cytosolic fractions. Confirming the imaging results, nuclear levels of wild-type or mutant HTTex1 were increased upon TBK1 coexpression (Fig EV3C and D). These observations show that TBK1-mediated phosphorylation of HTT increased its nuclear localization, in line with previous reports (Thompson *et al*, 2009; Atwal *et al*, 2011).

Previous studies indicated that phosphorylation or the introduction of phosphomimetic mutations at both S13 and S16 (Gu *et al*, 2009; Arbez *et al*, 2017; Branco-Santos *et al*, 2017; Chiki *et al*, 2017; Deguire *et al*, 2018) suppress mutant HTT aggregation *in vitro* and in cellular models. However, the effects of *bona fide* phosphorylation on mutant HTTex1 aggregation were evaluated only *in vitro* using semisynthetic proteins (Gu *et al*, 2009; Daldin *et al*, 2017; Deguire *et al*, 2018). Therefore, we tested whether TBK1-induced phosphorylation influences the aggregation of mutant HTT in HEK293 cells. We used HTTex1 72Q eGFP as a surrogate model of mutant HTT aggregation because the overexpression of this protein has consistently been shown to lead to extensive inclusion formation in different mammalian cells (Arrasate *et al*, 2004). We coexpressed either phosphorylation-deficient T3A and S13/S16A or phosphorylation-competent HTTex1 containing 72Q or 16Q repeats with TBK1 in HEK293 cells for 48 h. Then, we performed a WB analysis of soluble protein extracts and a filter retardation assay to assess the level of aggregated mutant HTT. In parallel, we also evaluated the number of TBK1-expressing cells presenting cytoplasmic and nuclear aggregates using ICC. Figure 3A and B show that TBK1 coexpression significantly reduced the levels of soluble wild-type or mutant HTTex1 in an HTT S13/S16 phosphorylation-independent manner, as evidenced by the decrease in the levels of HTTex1

mutants in which phosphorylation at T3 (T3A) or S13/S16 (S13A/S16A) was prevented by mutation to alanine (Fig 3A and B). Interestingly, we observed a stronger effect for TBK1 than for IKKβ on lowering the levels of soluble wild-type and mutant HTTex1. The filter retardation assay also showed a phosphorylation-independent reduction in HTTex1 72Q aggregates in the insoluble cellular fractions (Fig 3C and D). Interestingly, we also observed that similar to TBK1, IKKβ could decrease HTTex1 levels and mutant HTTex1 aggregates in a phosphorylation-independent manner (Fig 3C and D). Using ICC, we observed that 35–45% of cells expressing phosphorylation-competent HTTex1 72Q or the phosphorylation-deficient mutants S13/S16A and T3A formed aggregates, whereas only ~10% of cells coexpressing the same constructs with TBK1 showed aggregate formation (Fig 3E and F). A similar reduction in aggregated mutant HTT levels was observed for the phosphorylation-deficient HTTex1 mutants S13A/S16A and T3A (Fig 3E and F). These results indicate that the TBK1-induced reduction of soluble HTTex1 and HTT aggregates could be mediated by mechanisms that do not require phosphorylation of N17 at S13.

HEK293T cells transfected with HTTex1 72Q showed the formation of nuclear HTTex1 aggregates in approximately 10% of cells at the indicated time point. Therefore, we further examined the effect of TBK1 coexpression on nuclear aggregates. We observed that TBK1 expression also reduced the level of nuclear aggregates formed by HTTex1 72Q eGFP (Fig 3G).

Next, we sought to determine whether the decrease in the levels of soluble and aggregated mutant HTTex1 was dependent on TBK1 kinase activity. To test this hypothesis, we coexpressed phosphorylation-competent HTTex1 72Q and phosphorylation-deficient S13/S16A or the T3A mutant with TBK1 or its TBK1 KD in HEK293 cells. WB analysis of soluble protein extracts and quantification of aggregated mutant HTT by a filter retardation assay showed that TBK1 but not TBK1 KD decreased the levels of both soluble and aggregated HTTex1 72Q (Fig EV3E and F). These results establish that TBK1 coexpression lowers HTT levels in an S13/S16 phosphorylation-independent manner, suggesting that TBK1 may be involved in regulating HTT clearance largely via other mechanisms.

To determine whether TBK1-induced reduction of HTT aggregate formation could be mediated by its interaction or phosphorylation of HTT aggregates or inclusions, we assessed whether TBK1 or IKKβ could phosphorylate *in vitro*-generated HTTex1 fibrils or mutant HTTex1 aggregates in cells. Toward this aim, we first assessed the ability of TBK1 and IKKβ to phosphorylate preformed HTTex1 43Q fibrils in an *in vitro* assay and monitored the extent of phosphorylation at S13 by filter retardation immunoblot and mass spectrometry analysis. Interestingly, we observed that neither TBK1 nor IKKβ could phosphorylate preformed HTTex1 43Q fibrils, suggesting that the S13 residue is not readily accessible in the fibrillar conformation or that the kinase does not interact with HTTex1 fibrils (Fig EV3G). We also did not observe any disaggregation or release of HTTex1 43Q monomers during the *in vitro* phosphorylation reaction as evidenced by the absence of change in the levels of HTTex1 43Q fibrils in the filter retardation assay (Fig EV3G).

To determine whether TBK1 could phosphorylate already formed HTT aggregates in cells, we expressed mutant HTTex1 72Q in HEK293 cells for 48 h. At this time point, ~40% cells showed mutant HTTex1 aggregates. Then, we transfected TBK1 and monitored the levels of soluble HTT, HTT aggregates, and pS13 HTT over time by WB and the filter retardation assay. First, we did not observe phosphorylation at S13 in the HTTex1 72Q aggregates retained in the filter retardation assay (Fig 3H). Second, there was no increase in the pS13 levels of HTT aggregates upon overexpression of TBK1 after HTT aggregate formation (Fig 3H). These observations suggest that TBK1 phosphorylates monomeric or soluble HTT but not fibrils or inclusions of mutant HTTex1 in a cellular context, consistent with the data obtained in our *in vitro* phosphorylation assays (Fig EV3G).

Next, we examined whether TBK1 expression enhances the clearance of aggregated forms of mutant HTT. Consistent with our observation in Fig 3A and B, we observed that soluble HTT levels were reduced and S13 phosphorylation was increased upon TBK1 expression at various time points (Fig 3H). The levels of HTT aggregates were not reduced upon TBK1 overexpression at any given time point, suggesting the limited role of TBK1 in the phosphorylation or clearance of mutant HTT aggregates once they were formed. We observed a decrease in soluble HTT, kinase levels, and HTT aggregates at late time points, possibly due to the transient transfection. Accordingly, when testing whether TBK1 could induce clearance of HTT inclusions by ICC, we observed no reduction in the number of HTT inclusions upon overexpression of TBK1 (Fig 3I). These results indicate that the TBK1-induced reduction in HTT levels and aggregate formation is mediated by TBK1 kinase activity-dependent processes that act at the level of soluble HTT or during the early stages of its oligomerization, before HTT fibrilization and inclusion formation.

It was previously shown that mutant HTT from HD mouse model-derived cells shows less phosphorylation at S13/S16 than wild-type HTT (Atwal *et al*, 2011) and that pS13 HTT levels in a mouse striatal cell HD model as well as in HD knock-in mice are lower relative to wild-type controls (Cariulo *et al*, 2019). To assess the role of phosphorylation in HTT pathology, we examined S13 phosphorylation levels in the brain of the zQ175 mouse model (Menalled *et al*, 2012). We extracted the detergent (Triton X-100)-soluble and insoluble protein fractions from 6-month-old homozygous zQ175 and heterozygous HD mice along with wild-type control mice and subjected these samples to filter retardation assays and WB. We observed very low levels of soluble HTT in homozygous zQ175 mice, and there were no significant differences in the levels of soluble or pS13 HTT between control and heterozygous mice, at least as detected by WB (Fig EV3H). Analysis of the insoluble protein fractions revealed high levels of HTT in homozygous zQ175 mouse samples. Consistent with our previous observations, the mutant HTT proteins in the insoluble protein fraction were devoid of any pS13-phosphorylated HTT (Fig EV3I). Together, these results combined with the previous observations that phosphorylation within N17 (pT3, pS13, pS16) inhibited mutant HTTex1 aggregation (Cariulo *et al*, 2017; Chiki *et al*, 2017; Deguire *et al*, 2018) indicate that reduced phosphorylation at these residues may facilitate HTT aggregation. In summary, our findings show that the TBK1-induced reduction in HTT levels and aggregation is mediated by its ability to promote the clearance or prevent the aggregation of monomeric or soluble HTT species, rather than by the phosphorylation and disaggregation of HTT fibrils or inclusions.

The expression of mutant HTT has been shown to induce cytotoxicity in neuronal models of HD (Atwal *et al*, 2011; Arbez *et al*, 2017). Having shown that TBK1 overexpression reduced mutant

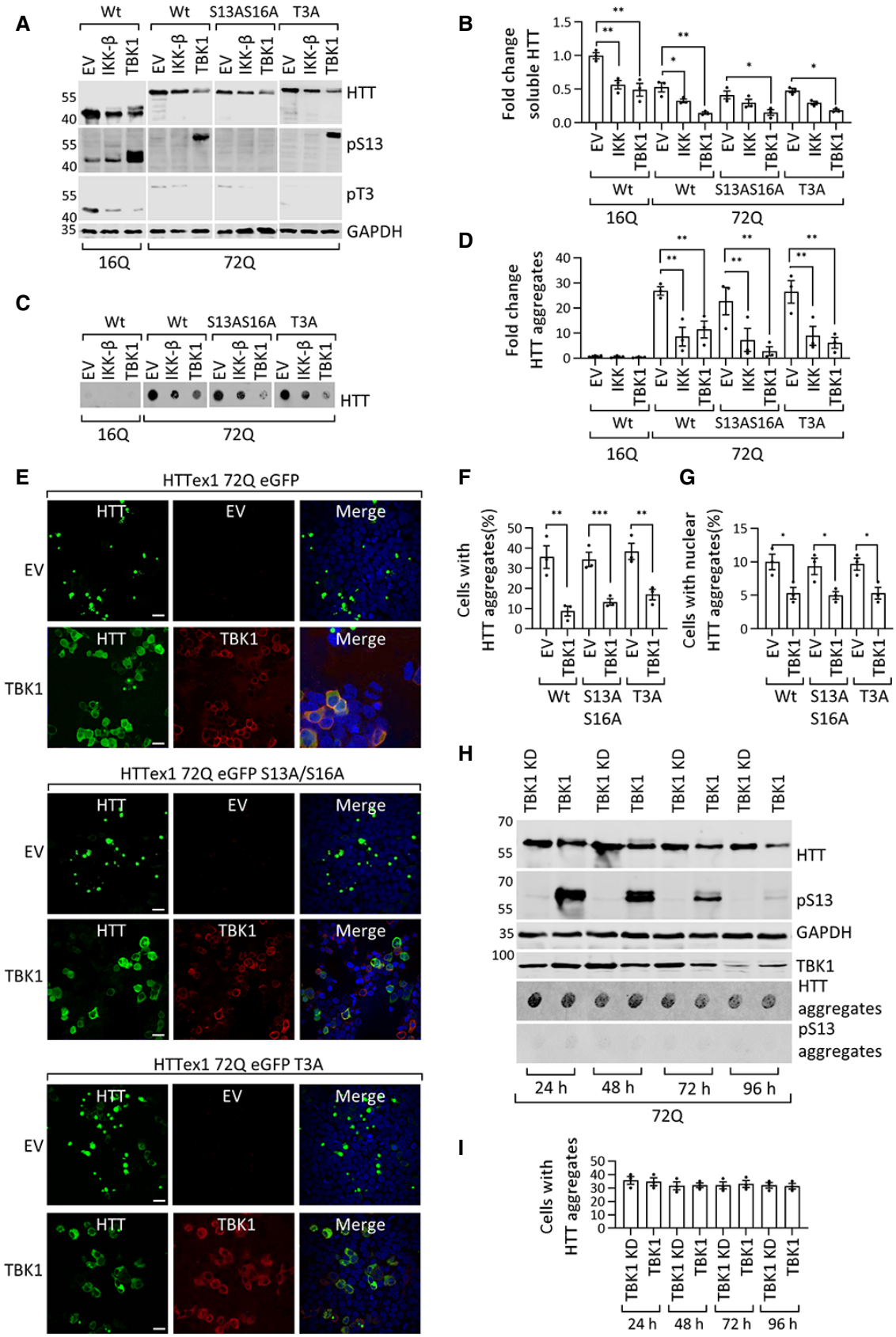

Figure 3.

Figure 3. TBK1 overexpression affects subcellular localization and reduces aggregation and cytotoxicity of HTT.

A Representative Western blot of soluble HTT (ab-MAB5492), HTT pS13 (ab-CHDI-90001039-1), and HTT pT3 (ab-CHDI-90001528-1) upon coexpression of HTTex1 16Q eGFP or 72Q eGFP or its phosphorylation-incompetent mutants with the indicated kinases for 48 h in HEK293 cells.

B The graph indicates the fold change in HTT in samples like illustrated in A, relative to empty vector controls normalized to GAPDH.

C Representative immunoblot of the HTT (ab-MAB5492) after filter retardation assay from the insoluble cellular fraction upon expression of HTTex1 16Q eGFP or 72Q eGFP or its phosphorylation-incompetent mutants with the indicated kinases for 48 h in HEK293 cells.

D Quantification of the fold change in HTT aggregates compared to EV expressing HTTex1 16Q from the experiments like in C.

E Representative immunofluorescence images of HTT aggregates (eGFP) and TBK1 (ab-anti-MYC) upon coexpression of HTTex1 72Q eGFP or its phosphorylation-incompetent mutants with the indicated kinases for 48 h in HEK293 cells (scale bar 20 μm).

F Quantification of the percentage of co-transfected cells presenting aggregates upon expression of the indicated kinase, from the experiments like in E.

G Quantification of the percentage of cells presenting nuclear aggregates from the experiments like in E.

H Representative Western blots of HTT (ab-MAB5492) and HTT pS13 (ab-CHDI-90001039-1) in soluble fraction and aggregates from HEK293 cells transfected first with HTTex1 72Q eGFP and then after 48 h (to enable the formation of aggregates before the kinase expression); with TBK1; cells were lysed at the indicated time after kinase transfection.

I Quantification of the percentage of cells presenting aggregates and kinase expression from the experiments in H.

Data information: Graphs report mean ± SEM, $n = 3$. Significance was assessed using 2-tailed Student's t-test, < 0.001***, 0.001 to 0.01**, 0.01 to 0.05*.
Source data are available online for this figure.

HTTex1 aggregates in HEK293 cells, we sought to determine whether this would also lead to suppression of mutant HTTex1-induced cytotoxicity. We used a previously established cytotoxicity (cell death) assay based on the measurement of nuclear condensation (Cummings & Schnellmann, 2004) during neuronal cell death induced by the expression of mutant HTT (Arbez *et al*, 2017). We co-transfected neurons with TBK1 or a TBK1 KD variant along with 16Q or 72Q HTTex1 or HTTN586 22Q or 82Q. Consistent with our previous studies (Arbez *et al*, 2017), we found that HTTex1 72Q or HTTN586 82Q expression induced significant cell death as assessed by nuclear condensation, compared to HTTex1 16Q or HTTN586 22Q (Fig 4A and B). TBK1 but not TBK1 KD coexpression partially rescued HTTex1 72Q- and HTTN586 82Q-induced toxicity (Fig 4A and B). We also observed a partial rescue of cell death induced by HTTex1 72Q upon TBK1 but not TBK1 KD coexpression in rat primary neuronal cultures using TUNEL assay (Fig 4C). To confirm the neuroprotection mediated by overexpression of TBK1 and the dependence on its kinase activity, we repeated the HTTN586 22Q and 82Q toxicity experiments in the presence of TBK1 kinase inhibitors. We observed that treatment with the TBK1 kinase inhibitor MRT68601 (McIver *et al*, 2012) blocked the neuroprotective effects induced by overexpression of TBK1 (Fig 4D). Next, we also tested whether the absence of TBK1 influences HTTex1 72Q-induced toxicity in *Tbk* $1^{-/-}$, *Tnf-α* $^{-/-}$ knockout (Hemmi *et al*, 2004) mouse primary striatal neurons. We observed increased toxicity in the absence of TBK1 (Fig 4E). These findings suggest that TBK1 expression or activation may represent a viable strategy to suppress mutant HTT-induced toxicity, whereas TBK1 inhibition may further exacerbate HTT toxicity.

TBK1 overexpression modulates HD pathology in *Caenorhabditis elegans*

Considering the ability of TBK1 to modulate HTT levels and its propensity to form cellular inclusions, we sought to determine whether overexpression of TBK1 could prevent mutant HTT aggregation and toxicity in a recently developed *C. elegans* model of HD (Lee *et al*, 2017). This model expresses the HTT N-terminal fragment up to residue 513 with 15 (Q15) or 128 glutamines (Q128) tagged with YFP in the muscle cells of the *C. elegans* body wall. In worms expressing HTTN513-YFP (Q15), HTT appeared soluble and diffusely localized to the cytosol, whereas HTT aggregates could be readily detected in the cytosol of the worms expressing mutant HTTN513-YFP (Q128) (Fig 5A). Using these *in vivo* models, we investigated the effect of TBK1 on mutant HTTN513 aggregation and toxicity. First, we assessed whether the N17 of HTTN513 was endogenously phosphorylated in *C. elegans*. To this end, we performed a biochemical analysis of protein lysates from this model with phospho-specific antibodies against HTT S13 and T3. We observed that worms expressing mutant HTTN513-YFP (Q128) showed less phosphorylation at T3 and S13 compared to worms expressing wild-type HTTN513-YFP (Q15) (Fig 5B and C), consistent with previous findings in animal models of HD and patient-derived cells (Aiken *et al*, 2009; Atwal *et al*, 2011; Cariulo *et al*, 2017, 2019). Importantly, the detection of pT3 and pS13 HTT in *C. elegans* indicates that this organism expresses kinases capable of phosphorylating HTT at these residues.

Approximately 81% of human kinases have orthologues in *C. elegans* (Manning, 2005; Lehmann *et al*, 2013). It was previously shown that transgenic overexpression of human kinases in *C. elegans* could be used to determine their effects on pathogenic disease mechanisms (Miyasaka *et al*, 2005; Branco-Santos *et al*, 2017). Therefore, we sought to determine the effect of the expression of human TBK1 in the muscle cells of the *C. elegans* HD model on HTTN513 phosphorylation, protein levels, and aggregation. We generated three different transgenic lines of HTTN513-YFP (Q15) and HTTN513-YFP (Q128) worms overexpressing TBK1 or TBK1 KD (fivefold to 15-fold) and quantified HTT levels, phosphorylation at S13, aggregate load, and worm motility, a functional phenotype affected by polyQ expansion in HTT (Lee *et al*, 2017). As shown in Fig 5D and E, we observed that all three lines of worms overexpressing TBK1 but not TBK1 KD showed increased phosphorylation of HTTN513-YFP at S13 in both the Q15 and Q128 models, with significantly reduced aggregate formation in the three different transgenic lines of the HTT513-YFP (Q128) model.

Expression of HTTex1 or HTTN513 with expanded polyQ in *C. elegans* muscle cells in the body wall leads to aggregation-related cytotoxicity, resulting in motility defects (Wang *et al*, 2006; Lee *et al*, 2017). Moreover, the HTTN513-YFP (Q128) *C. elegans*

model was shown to exhibit sustained mutant HTT-mediated toxicity and motility defects irrespective of the age of the worms (Lee *et al*, 2017). Therefore, we next assessed the effect of TBK1 on mutant HTT-induced toxicity and motility defects in this model. We examined the motility of HTTN513-YFP Q15 and Q128 worms coexpressing TBK1 or TBK1 KD in three transgenic lines. As

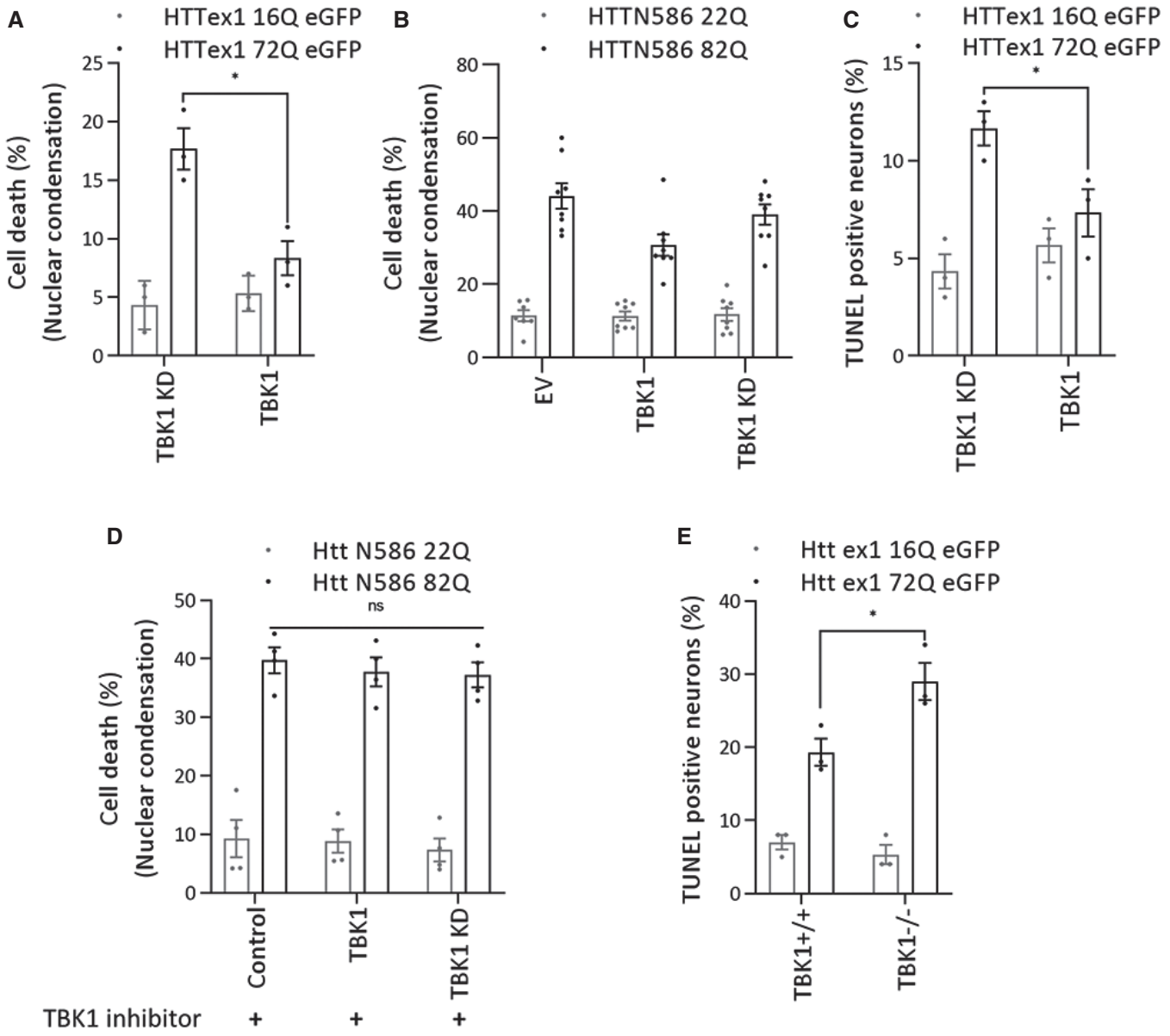

Figure 4. TBK1 expression leads to suppression of mutant HTT induced cytotoxic effects.

A, B Quantification of cell death by a nuclear condensation assay, cells were fixed and the nuclei were stained with Hoechst dye, and cells with a nuclear intensity higher than the average intensity plus two standard deviations are considered dead. (A) The percentage of cell death at DIV14, after co-transfection of indicated kinases and HTTex1 plasmid in rat primary striatal neurons at DIV9 (n = 3), (B) The percentage of cell death at DIV7, after co-transfection of indicated kinases and HTT N586 plasmid in mouse primary striatal neurons at DIV5 (n = 8).

C Quantification of cell death by a TUNEL assay in rat primary striatal neurons transfected with the indicated kinases at DIV9 with the indicated HTT plasmid. The cells were fixed at DIV14, and the percentage of TUNEL-positive neurons was counted and plotted (n = 3).

D The percentage of cell death, quantification by a nuclear condensation assay in mouse primary cortical neurons co-transfected with the indicated HTT N586 and kinases at DIV5, and cells were treated with TBK1 inhibitor MRT 68601 at DIV5 till DIV7. Cells were fixed, and the nuclei were stained with Hoechst dye (n = 3). (E) Quantification of cell death by a TUNEL assay in mouse primary striatal neurons transfected with the indicated kinases at DIV9 with the indicated HTT plasmid. The cells were fixed on DIV14, and the percentage of TUNEL-positive neurons was counted and plotted (n = 3).

Data information: Graphs report mean ± SEM. Significance was assessed using 2-tailed Student's t-test, 0.01 to 0.05*, ≥ 0.05 ns.
Source data are available online for this figure.

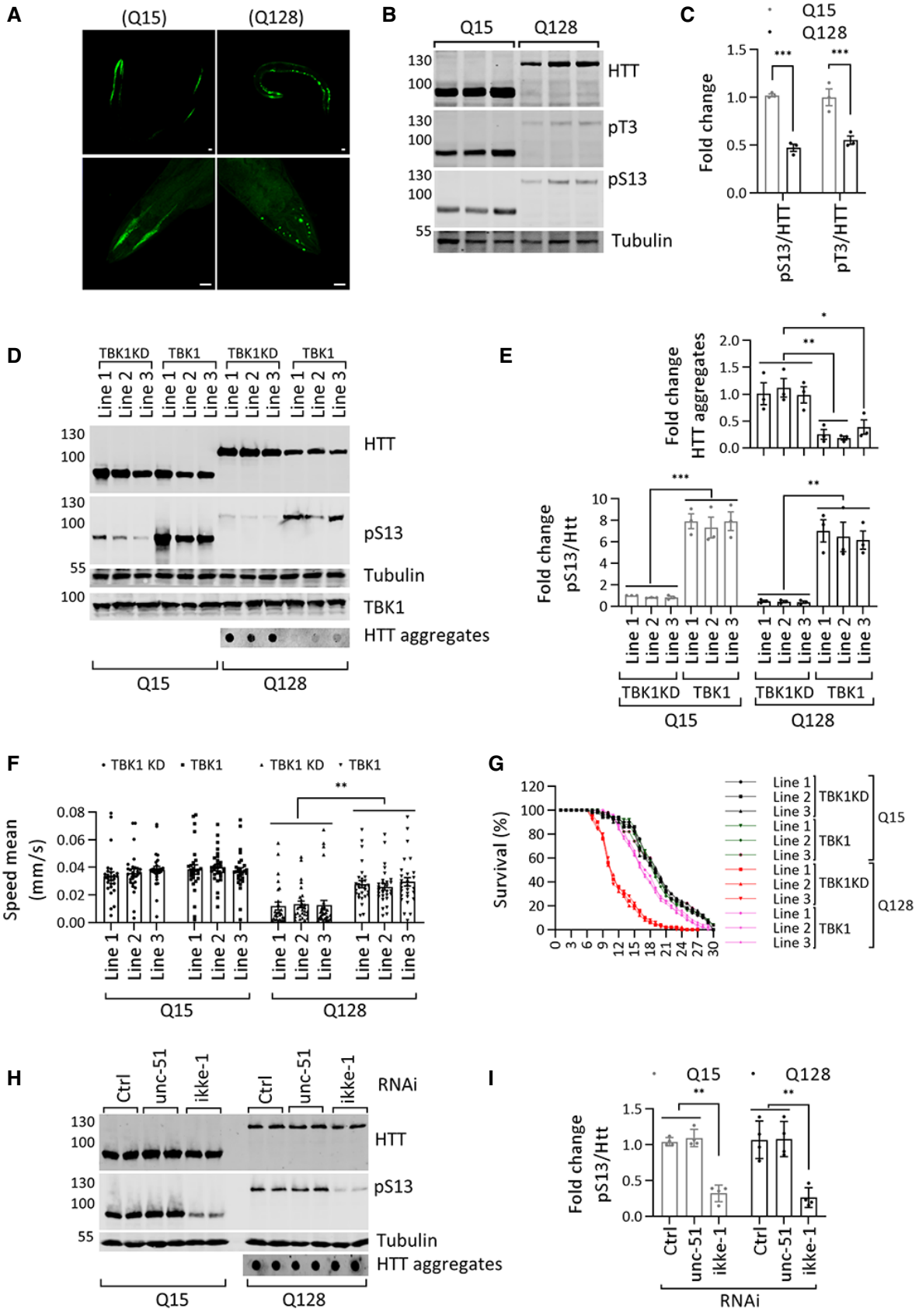
A
(Q15)
(Q128)
B
Q15
Q128
HTT
pT3
pS13
Tubulin
C
Q15
Q128
Fold change
pS13/HTT
pT3/HTT
D
TBK1KD
TBK1
Line 1
Line 2
Line 3
HTT
pS13
Tubulin
TBK1
HTT aggregates
Q15
Q128
E
Fold change
HTT aggregates
Fold change
pS13/Htt
TBK1KD
TBK1
Q15
Q128
F
TBK1 KD
TBK1
Speed mean
(mm/s)
G
Survival (%)
Q15
Q128
H
Ctrl
unc-51
ikke-1
RNAi
HTT
pS13
Tubulin
HTT aggregates
I
Fold change
pS13/Htt

Figure 5.

Figure 5. TBK1 overexpression modulates HD pathology in *C. elegans*.

A Representative immunofluorescence image of *C. elegans* overexpressing HTT N513 Q15 and HTT N513 Q128 (scale bar 20 μm). Top panel complete worm, lower panel head region.

B Western blot showing HTT (ab-MAB5492), HTT pS13 (ab-CHDI-90001039-1), and HTT pT3 (ab-CHDI-90001528-1) levels in *C. elegans* overexpressing HTT N513 Q15 and HTT N513 Q128.

C Quantification of the fold changes in ratios of HTT pS13 and pT3 to total HTT in *C. elegans* overexpressing HTT N513 Q15 and HTT N513 Q128 from the experiments like in B (n = 3).

D Representative Western blots showing the HTT (ab-MAB5492) and HTT pS13 (ab-CHDI-90001039-1) levels from the detergent soluble fraction and HTT aggregates (ab-MAB5492) from the detergent-insoluble fraction in three different transgenic *C. elegans* lines overexpressing TBK1 or the TBK1 KD.

E The bottom graph indicates the fold change in the HTT pS13 (ab-CHDI-90001039-1) ratios to total HTT (ab-MAB5492) compared to those in the kinase-dead mutant line 1 from the experiments like in D. The top graph indicates the fold change in HTT aggregates (ab-MAB5492) compared to that in the kinase-dead mutant the experiments like in D (n = 3).

F Mobility of the Q15 and Q128 *C. elegans* lines upon overexpression of TBK1 or TBK1 KD (n = 26–29).

G Survival graph of the Q15 and Q128 *C. elegans* lines upon overexpression of TBK1 or TBK1 KD (n = 30).

H Representative Western blots showing HTT (ab-MAB5492) and HTT pS13 (ab-CHDI-90001039-1) from the detergent soluble fraction and HTT aggregates (ab-MAB5492) from the detergent-insoluble fraction in TBK1 orthologue (ikke-1 or unc-51) RNAi-treated *C. elegans* lines expressing HTT N513 Q15 and HTT N513 Q128.

I Quantification of the fold change in the ratio of pS13 HTT to total HTT compared to non-targeting RNAi from the experiments like in H (n = 4).

Data information: Graphs report mean ± SEM. Significance was assessed using 2-tailed Student's t-test, < 0.001—except for (F) where 2-way ANOVA with Sidak post-hoc test was used. ***0.001 to 0.01**, 0.01 to 0.05*.
Source data are available online for this figure.

shown in Fig 5F, there was no significant difference in motility between worms coexpressing TBK1 or TBK1 KD with HTTN513-YFP (Q15). In contrast, the motility defect observed in worms expressing HTTN513-YFP (Q128) was significantly rescued upon coexpression of TBK1 but not the TBK1 KD mutant (Fig 5F). These results suggest that TBK1 coexpression suppresses mutant HTT-induced toxicity.

Overexpression of HTTN513 Q128 within muscle cells in the body wall of *C. elegans* was shown to impair their muscle function and shorten their lifespan (Lee *et al*, 2017). Therefore, we examined the lifespan of HTT N513 Q15 and Q128 worms coexpressing TBK1 or TBK1 KD in three different transgenic lines. As shown in Fig 5G, all three lines coexpressing TBK1 KD with HTTN513-YFP (Q128) displayed a shortened lifespan (mean lifespan of ~10 days) compared to that of three different lines coexpressing TBK1 KD with HTTN513-YFP (Q15) (mean lifespan of ~19 days). We observed that coexpressing TBK1 in HTTN513-YFP (Q128) worms suppressed the lifespan defect in all three lines (mean lifespan of ~17 days) (Fig 5G). These results show that TBK1 overexpression led to a significant reduction in mutant HTT aggregation and rescued mutant HTT-induced toxicity in *C. elegans*.

Next, we asked whether worm orthologues of TBK1 were involved in phosphorylating HTT at residue S13 in worms. Therefore, we tested the effect of downregulating the activity of the worm orthologues of TBK1 on HTT phosphorylation and aggregation. The worms were fed siRNAs targeting the TBK1 orthologues ikke-1 and unc-51 for 5–6 days. RT–PCR analysis of RNA from treated animals showed an efficient knockdown of their target kinases (Appendix Fig S2). We observed that knockdown of ikke-1 decreased pS13 levels in HTTN513-YFP (Q15) and HTTN513 -YFP (Q128) worms (Fig 5H and I) but had no significant effect on the levels of total HTT or HTT aggregates in the Q128-expressing model. These findings suggest that at least one of the *C. elegans* TBK1 orthologues, namely ikke-1, contributes to pS13 HTT levels in these transgenic animals, thus further validating TBK1 as one of the kinases regulating phosphorylation of HTT at S13 *in vivo*.

TBK1-induced reduction of HTTex1 72Q aggregates is dependent on autophagy

Our observation that TBK1 overexpression resulted in the reduction of HTTex1 levels and inclusion formation, independent of its ability to phosphorylate the protein suggests that TBK1 plays a role in regulating the degradation of soluble HTT. TBK1 is known to play key roles in autophagy, including the phosphorylation of several autophagy adaptors, which enhances their ability to engage LC3-II and ubiquitinated cargo (Weidberg *et al*, 2011; Kiriyama & Nochi, 2015; Ahmad *et al*, 2016; Richter *et al*, 2016) and to promote autophagosome maturation (Pilli *et al*, 2012; Oakes *et al*, 2017). To determine whether the TBK1-induced reduction in HTT levels was mediated by proteasome- or autophagy-related mechanisms, we assessed the effects of proteasome and autophagy inhibitors on HTT levels and aggregation in HEK293 cells coexpressing HTTex1 72Q with TBK1 or a TBK1 KD mutant. As shown in Fig 6A and B, we observed that autophagy/lysosome inhibitors but not proteasome inhibitor blocked the TBK1-mediated reduction of both soluble and aggregated forms of HTTex1 72Q (Fig EV4A).

To determine whether TBK1 overexpression could increase autophagy, we overexpressed TBK1 or TBK1 KD in HEK293 cells and primary neuronal cells and assessed the autophagic flux by monitoring changes in the levels of LC3B (Klionsky *et al*, 2016) in the cell lysates. We observed that TBK1 expression increased LC3B-II levels compared to TBK1 KD (Fig 6C and D). Bafilomycin A1 treatment resulted in a further increase in LC3B-II levels, consistent with this kinase's ability to increase autophagy (Fig 6C and D). An increase in autophagic flux is usually accompanied by increased clearance of the autophagy receptor p62 (Klionsky *et al*, 2016). Hence, we assessed p62 levels in TBK1 and TBK1 KD-expressing HEK293 cells and observed a significant decrease in p62 levels upon TBK1 overexpression compared to TBK1 KD (Fig EV4B and C). In primary striatal neuronal cultures, the expression of TBK1, but not TBK1 KD, resulted in a significant increase in LC3B-II levels (Fig 6E and F), with an associated decrease in p62 levels (Fig EV4D and E), indicating that TBK1

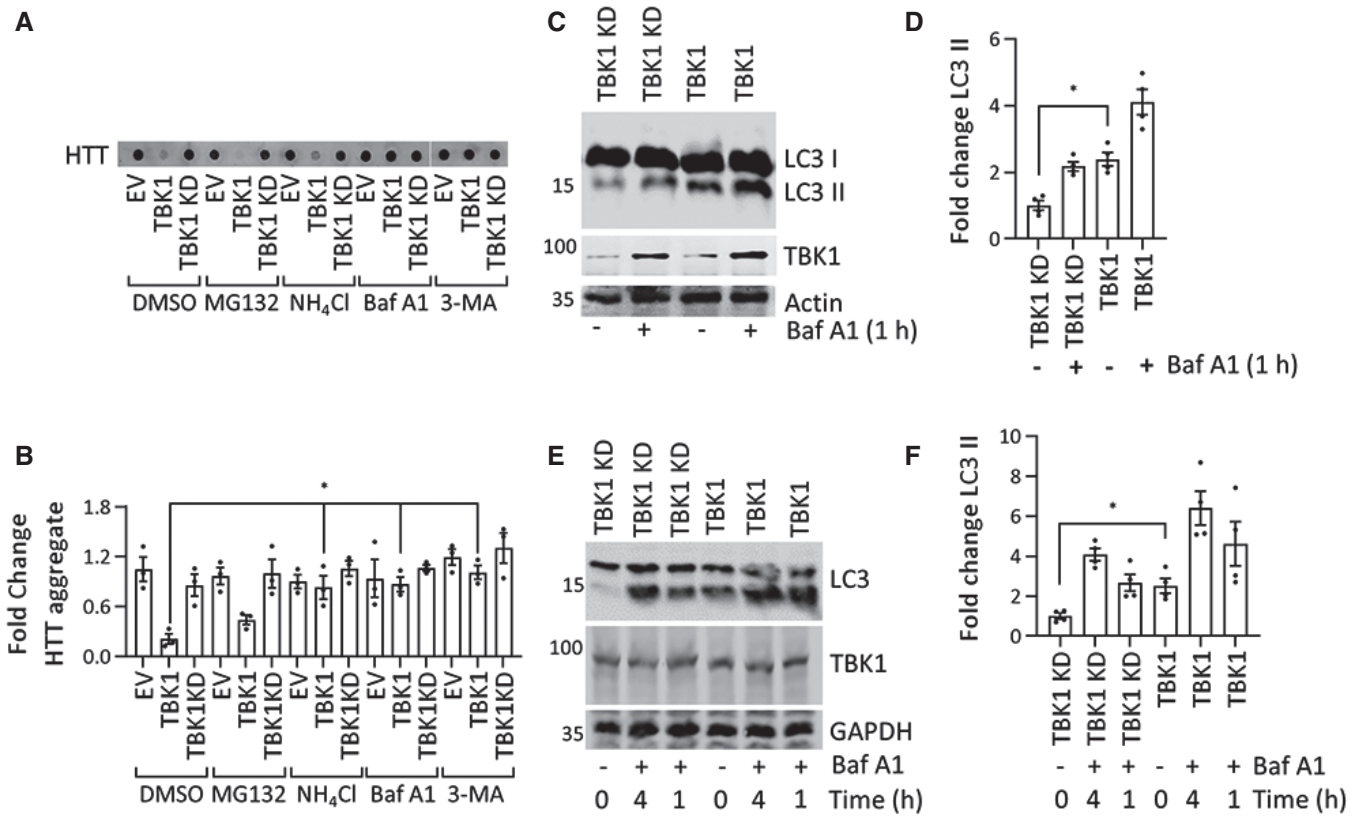

Figure 6. Autophagy inhibition blocks the HTTex1 72Q aggregate-reducing effect of TBK1.

A Representative immunoblot of a filter retardation of HTT (ab-MAB5492) from the insoluble cellular fraction; HEK293 cells coexpressed HTTex1 72Q eGFP and TBK1 or TBK1 KD for 48 h, and for the last 16 h, they were treated with the indicated proteasome inhibitor (MG132, 5 μM) or autophagy inhibitor (Baf A1, 200 nM, NH_4Cl, 10 mM, 3-MA,5 mM).

B Quantification of the fold change in HTT aggregates compared to TBK1 KD treated with DMSO from the blots like in A (n = 3).

C Immunoblot of LC3 (ab48394) from soluble HEK293 cellular fractions overexpressing TBK1 or TBK1 KD for 24 h; for the last hour, Baf A1 (500 nM) was added as indicated.

D Fold change in LC3-II levels (lower band) relative to the respective untreated kinase-dead mutant normalized to actin from the blots like in C (n = 3).

E Immunoblot of LC3 (ab48394) from soluble rat primary neuronal cells overexpressing lentivirus-mediated TBK1 and TBK1 KD for 96 h. For the last 1 or 4 h, Baf A1 (500 nM) was added as indicated.

F Quantification of the fold change in LC3-II levels (lower band) compared to the kinase-dead mutant, which was untreated, normalized to GAPDH from the blots like in E (n = 3).

Data information: Graphs report mean ± SEM. Significance was assessed using 2-tailed Student's t-test, 0.01 to 0.05*.
Source data are available online for this figure.

overexpression could increase autophagy in neuronal cells in a catalytic activity-dependent manner.

TBK1 was reported to phosphorylate the autophagy receptors optineurin (OPTN) and p62 (SQSTM1), ubiquilin-2, and the autophagy regulator RAB8B (Richter *et al*, 2016). Once phosphorylated, autophagy adaptors bind to ubiquitinated substrates and target these substrates for autophagy (Richter *et al*, 2016; Oakes *et al*, 2017). To validate the observed TBK1-mediated autophagy-inducing effects, we assessed whether HTT, TBK1, and autophagy adaptors co-localize in primary neurons by immunocytochemistry. We observed that endogenous, active TBK1 (phospho-serine 172; Richter *et al*, 2016) co-localized with HTT, LC3B, and ubiquitin in a subpopulation of punctate structures (Fig EV4F and G). We also observed that active TBK1 co-localized with the autophagy adaptor p62 in a few puncta in the cytosol (Fig EV4H and I). Taken together, our data suggest that TBK1 expression promotes the general cellular clearance mechanism of soluble HTT and prevents its accumulation and aggregation by enhancing autophagy.

Upon disruption of TBK1 binding to autophagy adaptor proteins, its effects on HTT levels and aggregate formation become strongly dependent on the phosphorylation state of HTT

To uncouple the effects of phosphorylation-dependent changes and TBK1-induced enhancement of autophagy on HTT turnover and aggregation, we investigated the effect of expressing a well characterized TBK1 mutant that is incapable of binding to autophagy adaptors (lacking amino acids 690–713, within the coiled-coil domain; Oakes *et al*, 2017). It has been shown that Δ690–713 TBK1 mutant could still phosphorylate known substrates, such as IRF3

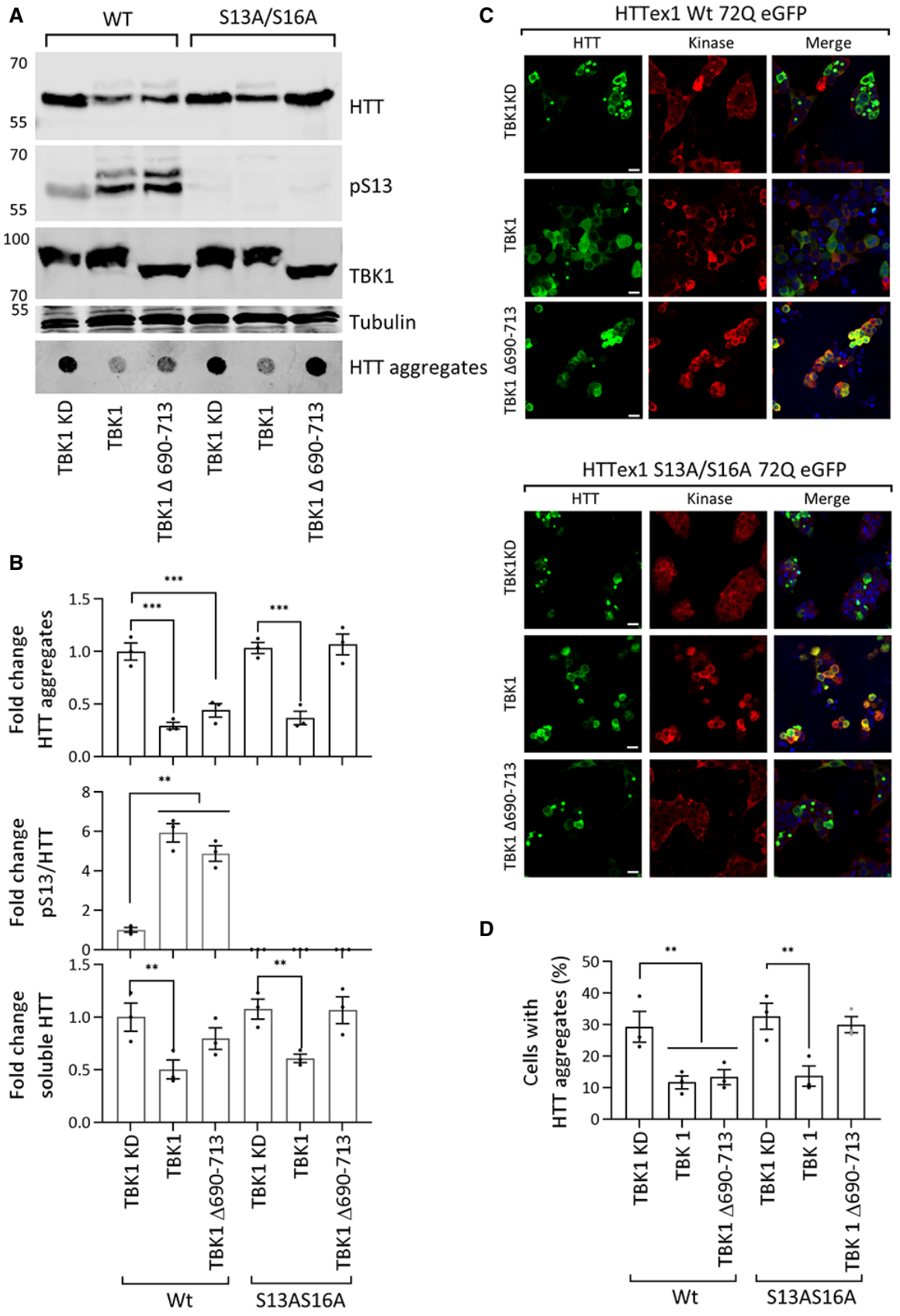

Figure 7.

Figure 7. TBK1 deficient in the autophagy adaptor-binding domain does not reduce HTTex1 72Q eGFP S13A/S16A aggregates.

A Western blot of soluble HTT (ab-MAB5492), HTT pS13 (ab-CHDI-90001039-1), and HTT aggregates (ab-MAB5492), upon coexpression of the HTTex1 72Q eGFP or HTTex1 72Q eGFP S13A/S16A variant with TBK1 KD, TBK1, or TBK1 Δ690–713 for 48 h in HEK293 cells.

B The graph indicates the calculated fold changes in HTT, HTT pS13 ratio to total HTT, and HTT aggregates all compared to the levels in TBK1 KD from the experiments like in A (bottom panel normalized to tubulin, $n = 3$).

C Representative immunofluorescence images of eGFP HTTex1 72Q or its phosphorylation-deficient variant S13A/S16A upon coexpression with TBK1 KD or TBK1 or TBK1 Δ690–713 (ab-anti-Myc) with for 48 h in HEK293 cells (scale bar 20 μm).

D The graph indicates the percentage of co-transfected cells presenting aggregates upon expression of the indicated kinase, from the experiments like in C ($n = 3$).

Data information: Graphs report mean ± SEM. Significance was assessed using 2-tailed Student's *t*-test, < 0.001***, 0.001 to 0.01**.
Source data are available online for this figure.

(Freischmidt *et al*, 2015, 2017). Next, we examined the effects of the expression of TBK1 Δ690–713, TBK1 wild type, or TBK1 KD on the levels and aggregation of phosphorylation-competent and phosphorylation-deficient S13A/S16A mutant HTTex1 72Q in HEK293 cells. Fig 7A and B shows that both TBK1 Δ690–713 and TBK1 wild type could phosphorylate HTTex1 72Q resulting in a significant reduction in HTTex1 72Q aggregates. However, blocking phosphorylation at S13 and S16 prevented the ability of TBK1 Δ690–713 to reduce HTTex1 72Q aggregation (Fig 7A–D). Unlike wild-type TBK1, coexpression of TBK1 Δ690–713 had minimal effects on the levels of soluble HTT. These results indicate that the TBK1-mediated reduction of mutant HTT aggregates was dependent on its autophagy adaptor-binding function and this mechanism was the primary contributor to the phosphorylation-independent reduction of HTT aggregates upon coexpression of TBK1. The removal of the 690–713 region interfered with the ability of TBK1 to phosphorylate p62 and OPTN, and its ability to activate autophagic flux (Fig EV4J). Under these conditions, TBK1 mediated effect on HTT aggregation was dependent on the phosphorylation state of HTT at S13/S16. Importantly, these data show that phosphorylation at S13 was sufficient to prevent mutant HTT aggregation in the absence of TBK1 mediated enhancement of autophagy and lowering of mutant HTTex1 levels. These results are consistent with our recent *in vitro* studies (Deguire *et al*, 2018) and previous studies using phosphomimetics (S13D/S16D) in a mouse model of HD (Gu *et al*, 2009) and cell lines (Thompson *et al*, 2009; Atwal *et al*, 2011; Branco-Santos *et al*, 2017).

TBK1 levels are not altered in R6/2 transgenic HD mouse model and HD patients brain

To determine whether the levels of TBK1 are altered in HD and HD models, we examined the levels of active TBK1 (phospho S172 = pS172) and total TBK1 in R6/2 transgenic HD mouse model, human postmortem brain tissues, and in HD patient brain tissue microarray (active TBK1 pS172). We observed no change in TBK1 or TBK1 pS172 levels in R6/2 transgenic HD mouse brain tissue lysates at time points up to 12 weeks (4, 8, 12 weeks) compared to age-matched wild type (Fig EV5D). Next, we obtained five HD and five non-HD postmortem cortical brain tissues and analyzed TBK1 level. We observed a trend of decrease in both the total and active TBK1 levels in these tissues, which was not statistically significant (Fig EV5E and F). This led us to examine the levels of both TBK1 and active TBK1 in a larger set of human samples. For this, we chose to use the tissue microarray approach. As shown in Fig EV5G and H, we did not observe any significant changes in active TBK1 pS172 levels in 21 HD samples compared with 18 control samples from the middle temporal gyrus tissue microarray (total TBK1 antibody was not suitable for immunohistochemistry on paraffin tissue microarrays). Moreover, there was no apparent correlation between the expression levels of active TBK1 and HTT stained by TBK1 pS172 and HTT 1C2 antibodies, respectively (Fig EV5I). These results suggest TBK1 levels may not be drastically changed in HD cases.

Discussion

Increasing evidence from *in vitro*, cellular, and animal model studies show that phosphorylation or mimicking phosphorylation at S13 and/or S16 attenuates mutant HTT aggregation and toxicity (Thompson *et al*, 2009; Atwal *et al*, 2011; Arbez *et al*, 2017; Branco-Santos *et al*, 2017; Deguire *et al*, 2018). However, whether inhibiting mutant HTT aggregation is the primary mechanism underlying the protective effects of phosphorylation at these residues remains unknown. This is in part because the majority of previous studies aimed at dissecting the role of S13/S16 phosphorylation in cellular and animal models were based primarily on approaches relying on the use of mutations to mimic or block phosphorylation, rather than *bona fide* phosphorylation and thus did not account for the dynamic nature of phosphorylation. To address this knowledge gap and elucidate the role of phosphorylation at S13 and S16 in HTT aggregation, turnover, and toxicity, we set out to identify kinases capable of increasing S13 HTT phosphorylation and identified TBK1 kinase.

Herein, we showed that TBK1 co-incubation with wild-type or mutant HTTex1 or longer N-terminal HTT fragments resulted in phosphorylation of both S13 and S16 (Figs 1C and EV1A and B). In contrast to IKKβ, which was shown previously to preferentially phosphorylate wild-type HTTex1 at residue S13 (Thompson *et al*, 2009). In our hands, IKKβ phosphorylated both S13 and S16, although much less efficiently than TBK1 (Fig EV2A and B). TBK1 possesses robust autophosphorylation and dimerization capacity (Oakes *et al*, 2017) that may lead to its high activation compared to IKKβ, which requires two other subunits for its full activation. This could also be one reason for the observed difference in the efficiency of the two kinases toward HTT S13 phosphorylation *in vitro*. TBK1 coexpression/overexpression robustly and efficiently increased S13 phosphorylation of both wild-type and mutant HTT in cells by approximately 5-fold to 10-fold compared to 3-fold to 4-fold by IKKβ (Fig 1D and E) and led to stronger HTT-lowering effects, especially for mutant HTTex1. To the best of our knowledge, this is the first report demonstrating that HTT is a substrate of TBK1. The discovery of TBK1 provides an efficient tool for manipulating HTT

phosphorylation levels in cells and enabled us to systematically determine how modulating phosphorylation at these residues influence HTT aggregation (Fig 8A), clearance, and toxicity in different models of HD.

TBK1 regulates the autophagy-mediated clearance of monomeric HTT

Our results demonstrate that TBK1 modifies HTT aggregation and toxicity through autophagy-mediated regulation of HTT clearance. TBK1 overexpression in cells reduced the levels of soluble HTTex1 and prevented the accumulation of mutant HTTex1 inclusions in a kinase activity-dependent manner, whereas TBK1 knockdown, knockout, or inhibition resulted in increased HTT levels. These observations suggest that TBK1 regulates mutant HTT levels and inclusion formation by activating clearance mechanisms such as proteasome- or autophagy-mediated protein clearance.

TBK1 levels and activity have been implicated in regulating many aspects of autophagy. For example, *TBK1* gene duplication in human iPSC-derived retinal cells or overexpression of TBK1 in RAW264.7 cells lead to increased LC3II and increased autophagy (Pilli *et al*, 2012; Ritch *et al*, 2014). TBK1-mediated phosphorylation of the autophagy adaptor proteins OPTN and p62 represents a rate-limiting step in the autophagic degradation of misfolded protein aggregates. Several studies have also shown that TBK1 acts as a scaffolding protein and plays an important role in regulating autophagic activity by regulating protein targeting to autophagosomes, autophagosome formation, autophagosome engulfment of substrates (Matsumoto *et al*, 2011; Korac *et al*, 2013), and fusion of autophagosomes to autolysosomes (Pilli *et al*, 2012). TBK1 depletion negatively impacts all of these processes and causes decreased autophagic activity (Oakes *et al*, 2017). Defects in autophagy and autophagosome formation and clearance have been implicated in the pathogenesis of neurodegenerative diseases (Nixon, 2013; Scrivo *et al*, 2018).

Consistent with its role in autophagy (Oakes *et al*, 2017), we observed that TBK1 was localized surrounding the HTTex1 inclusions in HEK293 cells and rat striatal primary neurons (Fig EV5A–C). TBK1 overexpression in HEK293 cells led to an increase in autophagic flux and the phosphorylation of the autophagy adaptors OPTN and p62 (Fig EV4J). To determine whether TBK1-mediated enhanced clearance or reduced aggregation of HTT was due to its interaction with and/or phosphorylation of HTT monomers, aggregates or both, we assessed the effect of TBK1 overexpression on HTT levels and aggregation in different HD models. Interestingly, we observed that TBK1-mediated reduction in HTT levels and aggregation were strongly dependent on TBK1 kinase activity and its ability to bind to the autophagy adaptor OPTN, but occurred independently of phosphorylation at S13 (Fig 8B). However, upon disruption of TBK1 interactions with the autophagy adaptors OPTN and p62, the effects of TBK1 on HTT levels and aggregation became strongly dependent on both its kinase activity and HTT phosphorylation at S13. These findings suggest that the primary mechanism underlying the beneficial effects of TBK1 is mediated by its ability to enhance autophagy, possibly through phosphorylation of the autophagy adaptors OPTN and p62 (Fig 8C). Preliminary studies from our group (Maharjan *et al*, unpublished) investigating the PTM-dependent interactome of soluble monomeric HTT showed that phosphorylation at S13 and S16 promoted interactions between mutant HTT and many autophagy, folding, and endocytic pathway components, suggesting that phosphorylation at these residues could also regulate HTT levels by promoting its interactions with key mediators of cellular proteostasis mechanisms. The proposed role of HTT as an autophagy scaffold protein (Ochaba *et al*, 2014) is also consistent with this hypothesis.

The aggregation inhibitory and protective effects of TBK1-mediated phosphorylation at S13 are consistent with previous findings demonstrating that reduction of HTT S13 phosphorylation by IKKβ knockout in striatum resulted in a significant increase in HTT levels in wild-type or R6/1 HD mouse (Ochaba *et al*, 2019) and further enhanced the behavior defect and increased neurodegeneration and microglial activation in R6/1 mice. We also previously showed that phosphorylation of mutant HTT at S13/S16 significantly reduced the helical propensity of N17 and the rate and extent of HTTex1 aggregation *in vitro* (Deguire *et al*, 2018). Together, these observations further support the hypothesis that enhancing phosphorylation at S13 is sufficient to induce a significant reduction in HTT levels, aggregation, and inclusion formation.

TBK1 does not phosphorylate or reduce preformed HTT aggregates or inclusions

Interestingly, TBK1 does not phosphorylate mutant HTTex1 fibrils *in vitro* or HTT in cellular inclusions and overexpression of TBK1 does not result in the clearance of mutant HTT aggregates once they were formed (Fig 8D). Whether TBK1 promotes the clearance of HTT monomers, oliogomers or both remains unknown. Unfortunately, the existing models of HTT aggregation and inclusion formation did not allow for investigating the effect of TBK1-mediated phosphorylation on early aggregation events and its effect on HTT oligomerization. HTT oligomers are usually short-lived and difficult to monitor and isolate from cells. Therefore, further studies are required to determine whether TBK1 acts on pre-fibrillar/inclusions intermediates and promote their autophagic clearance. Our observation that TBK1 was not able to induce the clearance of HTT post-aggregation is consistent with previous studies showing that autophagy induction by rapamycin treatment had no effect on the levels of HTT aggregates once mature aggregates were formed but reduced HTT aggregate formation and cell death when applied at the earlier stages of the aggregation process (Ravikumar *et al*, 2002). Together, these findings suggest that the beneficial effects of TBK1 are mediated by its activity-dependent regulation of the phosphorylation and degradation of monomeric or soluble forms, but not aggregated forms of HTT.

These observations also suggest that the N17 domain adopts a different conformation in the aggregated state of mutant HTT and/or that TBK1 does not interact with aggregated forms of HTT. Indeed, previous solid-state NMR studies on HTTex1 fibrils showed that N17 was less mobile and engaged in interactions with the amyloid core or PRD domain in the fibrillar state (Fig 8A; Bugg *et al*, 2012; Lin *et al*, 2017). The inaccessibility of N17 in the fibril state suggests that post-aggregation phosphorylation or potentially other PTMs in the N17 domain N17 are less likely to occur post-aggregation (Fig 8D). These findings imply that the N17 PTM-dependent regulation of HTT aggregation and clearance is likely

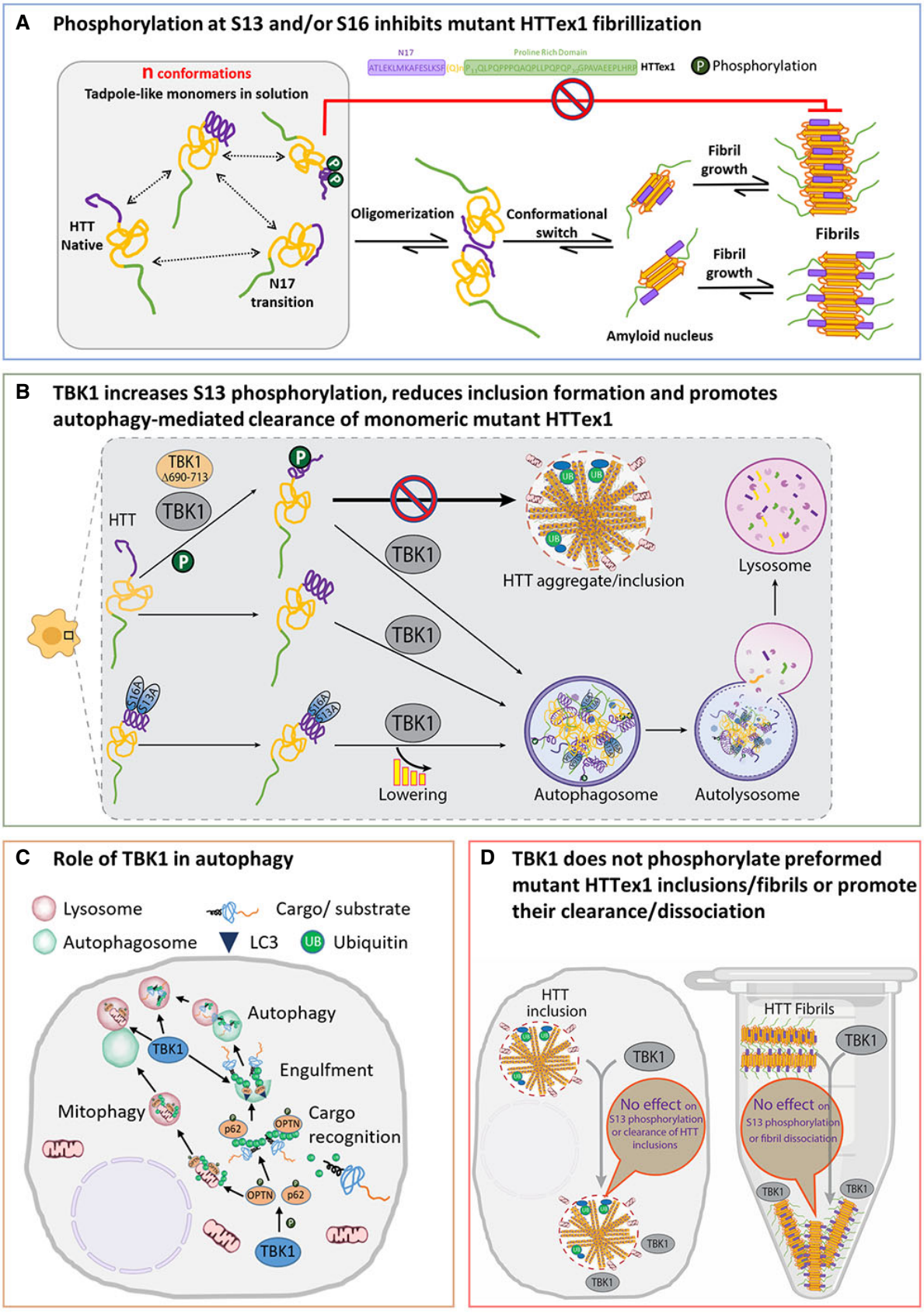
A
Phosphorylation at S13 and/or S16 inhibits mutant HTTex1 fibrillization
N17
Proline Rich Domain
HTTex1
Phosphorylation
n conformations
Tadpole-like monomers in solution
HTT Native
N17 transition
Oligomerization
Conformational switch
Fibril growth
Fibrils
Fibril growth
Amyloid nucleus
B
TBK1 increases S13 phosphorylation, reduces inclusion formation and promotes autophagy-mediated clearance of monomeric mutant HTTex1
TBK1 Δ690-713
TBK1
HTT
HTT aggregate/inclusion
Lysosome
Lowering
Autophagosome
Autolysosome
C
Role of TBK1 in autophagy
Lysosome
Cargo/ substrate
Autophagosome
LC3
Ubiquitin
Autophagy
Engulfment
Mitophagy
Cargo recognition
D
TBK1 does not phosphorylate preformed mutant HTTex1 inclusions/fibrils or promote their clearance/dissociation
HTT inclusion
No effect on S13 phosphorylation or clearance of HTT inclusions
HTT Fibrils
No effect on S13 phosphorylation or fibril dissociation

Figure 8.

Figure 8. Schema of the effect of HTT phosphorylation and TBK1 on aggregation.

A Effect of S13 and/or S16 phosphorylation on HTTex1 aggregation. HTTex1 forms a tadpole-like monomer structure, and N17-driven interaction may further drive HTTex1 oligomerization and fibril formation. Phosphorylation at S13 and S16 destabilizes the helix at N17 that leads to inhibition of the formation of HTTex1 fibrils.

B Effect of TBK1 on HTT in the cellular HD model. TBK1 and TBK1 Δ690–713 both phosphorylate monomeric or soluble HTTex1 72Q at S13 residue leading the reduction of the aggregation, but TBK1 also reduces the aggregation of both HTTex1 and HTTex1 S13A/S16A through the lowering of the HTT levels at the monomeric stage by enhancing the autophagic degradation. TBK1 Δ690–713 only reduces the aggregation of phosphorylation-competent HTTex1 but does not reduce the aggregation of HTTex1 S13A/S16A highlighting the role of S13 phosphorylation in aggregation inhibition.

C TBK1 effects on different stages of autophagy. TBK1 is known to phosphorylate autophagy adaptors p62 and OPTN that bind ubiquitinated substrates like proteins or damaged mitochondria and recruit LC3 and increase the autophagic clearance of substrates.

D TBK1 does not phosphorylate HTTex1 in inclusion/fibrils or promote their clearance/disaggregation. When HTT was already aggregated in cells or when in fibril form *in vitro*, possibly S13 residue is not accessible for TBK1 phosphorylation as N17 was shown to be collapsed on fibrillar core or it is near the core. Also, TBK1-mediated autophagy flux was not able to induce the lowering of HTTex1 inclusion. There was no disaggregation of fibrils up on TBK1 kinase *in vitro*.

mediated by the aggregation inhibitory effects of PTMs at the monomer level or their ability to selectively target monomeric or soluble HTT species for degradation. Several lines of evidence support this hypothesis: (i) We failed to detect phosphorylation at S13 in insoluble HTT fractions and aggregates from cellular and animal models of HD, whereas phosphorylation at S13 was readily detectable in the soluble fractions; (ii) several studies reported reduced phosphorylation at T3 and S13/S16 on mutant HTT compared to wild-type HTT in cell, mouse, and HD patient iPSC derived models (Aiken *et al*, 2009; Atwal *et al*, 2011; Cariulo *et al*, 2017); and 3) previous and recent studies from our group showed that the majority of the N17 modifications at the monomeric level (phosphorylation at T3, S13, S16, and S13/S16; ubiquitination; SUMOylation; methionine oxidation) inhibit mutant HTTex1 aggregation (Steffan *et al*, 2004; Thompson *et al*, 2009; Chiki *et al*, 2017; Deguire *et al*, 2018).

Therapeutic implications

The discovery of TBK1 as a kinase that efficiently phosphorylates HTT at S13 presents unique opportunities to directly assess the effect of phosphorylation at these residues and/or selective autophagic degradation of monomeric HTT as therapeutic targets for the treatment of HD. Several lines of evidence support the feasibility of these approaches: (i) Small molecules such as GM1 (Di Pardo *et al*, 2012) and N6-furfuryladenine (Bowie *et al*, 2018) were shown to increase S13/S16 phosphorylation and restore normal motor behavior in the YAC128 HD mouse model; (ii) a BACHD mouse model expressing S13D/S16D HTT showed reduced aggregate formation and suppression of HD pathology, such as motor deficits (Gu *et al*, 2009); (iii) in cellular models, HTTex1 S13D/S16D levels were reduced compared to HTTex1 (Thompson *et al*, 2009); and (iv) our results in *C. elegans* showed that TBK1-mediated increased phosphorylation at S13 resulted in a significant reduction of HTT aggregates and improved worm lifespan and motility. Furthermore, we showed that increasing TBK1 levels or activity resulted in a robust increase of HTT phosphorylation and enhancement of autophagy, leading to reduced HTT levels and suppression of HD pathology and toxicity, suggesting that targeting TBK1 represents a viable strategy for the treatment of HD.

Increasing evidence suggests that dysfunction in autophagy and other protein clearance mechanisms play central roles in the pathogenesis of neurodegenerative diseases, including HD (Nixon, 2013). HTT has also been demonstrated to function as a scaffold protein for selective macroautophagy and to promote selective autophagy through its ability to interact with p62 and ULK1 simultaneously, thus suggesting a role in both cargo recognition efficiency and autophagosome formation initiation (Ochaba *et al*, 2014; Rui *et al*, 2015). Herein, we showed that TBK1 expression/activation helped to overcome the autophagy defects induced by HTT misfolding and aggregation in HD models. Our data suggest that TBK1 expression/activation increases the phosphorylation of the cargo/substrate recognition adaptors OPTN and p62. Phosphorylation of OPTN or p62 was shown to facilitate the autophagy-dependent clearance of damaged or dysfunctional mitochondria (Matsumoto *et al*, 2015; Richter *et al*, 2016), and misfolded proteins and aggregates of proteins linked to neurodegenerative diseases, such as mutant SOD1 (Korac *et al*, 2013) and HTT (Matsumoto *et al*, 2011). TBK1-mediated enhancement of cargo/substrate recognition by the adaptors OPTN and p62, and *OPTN* mRNA levels were shown to be partially reduced in HD patient brain tissues (Hodges *et al*, 2006). In cellular models of HD (expressing HTTex1 103Q), OPTN knockdown led to an increase in HTT aggregation (Korac *et al*, 2013). Although the role of OPTN in the progression of HD is currently unknown, reducing OPTN activity or levels may confer susceptibility to HTT aggregation because of its role in autophagic clearance of protein aggregates. Therefore, pharmacological enhancement of the TBK1 pathway could activate the available pool of OPTN, which may, in turn, increase the recognition and clearance of HTT. Previous studies suggested that general autophagy induction in HD mouse models reduces aggregate load and improves motor performance and lifespan (Ravikumar *et al*, 2004; Tanaka *et al*, 2004; Rose *et al*, 2010). Our results suggest that TBK1 is a strong candidate for activating specific steps involved in the autophagy cascade (Fig 8D), and for the reduction of the autophagy substrates.

Although increasing TBK1 activity represents an attractive strategy for lowering the levels of soluble HTT species and preventing HTT aggregation, our findings showed that TBK1 did not act on or promote the phosphorylation or degradation of preformed HTT aggregates. However, given the dynamic nature of HTT aggregation and its reversibility (Yamamoto *et al*, 2000; Regulier *et al*, 2003), for example, under conditions where HTT expression was suppressed or lowered, it is likely that the TBK1-mediated reduction in soluble HTT could significantly contribute to a reduction in the levels of HTT aggregate formation by means of preventing the growth of existing aggregates and/or the formation of new aggregates. Our current data and previous observations by Ravikumar *et al* (2002) suggest that early activation of autophagy could be beneficial and promote the clearance of mutant HTT aggregates in HD. One consideration is that with

increasing age and at advanced disease stages, autophagy-lysosome and proteasome abnormalities become more apparent in HD (Seo *et al*, 2004; Cortes & La Spada, 2014). However, given that patients with HD can be identified at pre-symptomatic disease stages through genetic testing, therapeutic autophagy modulation alone or in combination with HTT-lowering strategies before disease onset is theoretically possible in HD and might be necessary for a significant beneficial effect.

Implications for other neurodegenerative diseases

Several stages of autophagy, such as substrate sequestration and autophagosome formation, autophagosome–lysosome–endosome fusion, and lysosomal digestion, were shown to be impaired in Amyotrophic lateral sclerosis (ALS), Alzheimer's disease (AD), Parkinson's disease (PD), and Frontotemporal dementia (FTD) (Nixon, 2013). Mutations in TBK1 and OPTN cause ALS and were shown to impair autophagy (Oakes *et al*, 2017). Targeting autophagy induction in these diseases by mTOR inhibitors, AMPK activation or selective autophagy induction by overexpression of specific genes has been shown to be beneficial in different cellular and mouse models of neurodegenerative diseases such as ALS, AD, PD, and FTD (Spilman *et al*, 2010; Wu *et al*, 2011; Qi *et al*, 2012; Oueslati *et al*, 2013; Menzies *et al*, 2017; Sorrentino *et al*, 2017; Scrivo *et al*, 2018). Considering the role of TBK1 in autophagy and the increasing evidence implicating its activity in the clearance of misfolded protein aggregates and ALS, it is plausible that pharmacological enhancement of TBK1 activity or selective targeting of TBK1-dependent autophagic pathways represents attractive and viable therapeutic strategies for the treatment of multiple neurodegenerative diseases, provided that TBK1 levels are not severely reduced in the disease. Indeed, we did not observe any changes in TBK1 and TBK1-pS172 in the brains of R6/2 transgenic HD mouse model and HD postmortem brain tissue (Fig EV5D–I). Recent success stories in finding kinase activators for Lyn, PKCδ, and AMPK kinase (Cool *et al*, 2006; Bessa *et al*, 2018) in the fields of diabetes drug development suggest that finding activators of TBK1 activity is feasible and may provide a therapeutic option to treatment of HD and other neurodegenerative diseases.

Materials and Methods

Antibodies and chemicals

The antibodies and chemicals used in the study are listed in Appendix Table S1, including the clone name, catalog numbers, commercial providers.

Plasmids and constructs

cDNAs encoding N-terminal HTT fragments (exon 1) bearing different polyQ lengths (Q16 or Q72) and HTT N548 were described previously (Bustamante *et al*, 2015). Myc-TBK1 plasmid (RC205238) and Myc-IKKβ plasmid (RC219154) were obtained from Origene, Rockville, MD, USA. TBK1 Δ690–713 was obtained by site-directed mutagenesis of RC205238 plasmid. Flag-TBK1 kinase-dead (K38A) plasmid (DU12696) was obtained from MRC PPU Reagents and Services, School of Life Sciences, University of Dundee. TBK1 lentiviral plasmid (LV330421) was obtained from Abmgood (Applied Biological Materials Inc.), Richmond, Canada. TBK1 KD (K38A) lentiviral plasmid was obtained by site-directed mutagenesis mutation to LV330421 plasmid. To get plasmids of TBK1 and TBK1 KD for *C. elegans* expression, TBK1 and TBK1 KD sequences were PCR-amplified from RC205238 and DU12696 and introduced to pPD30_38 (Addgene Plasmid #1443).

In vitro phosphorylation of HTTex1 with TBK1 and IKKβ

HTTex1 proteins were expressed, purified, disaggregated, and prepared for phosphorylation as we previously described (Reif *et al*, 2018). After the disaggregation of HTTex1 and evaporation of any residual TFA acid, the protein was dissolved at a final concentration of 0.5 mg/ml, in the phosphorylation buffer: 50 mM Tris, 25 mM $MgCl_2$, 8 mM EGTA, 4 mM EDTA, and 1 mM DTT (this solution is to be freshly prepared each time). Next, the pH of the reaction was adjusted to 7.4, and 5 mM Mg-ATP was added to the reaction solution, as well as purified recombinant TBK1 or IKKβ (# DU12469, #DU3167—MRC PPU Reagents and Services, University of Dundee) at a ratio of 1 μg of kinase per 30 μg of protein. The reaction mixture was kept at 30°C and monitored over time by mass spectroscopy (LC-ESI-MS) and Western blot (WB). To perform the mass spectroscopy, 5 μl of the reaction mixture was injected in the Thermo Scientific LTQ ion trap. To obtain the intact molar mass, the different charge states were deconvoluted using MagTran software. Additionally, 10 μl of the kinase reaction solution was supplemented with 2× Laemmli loading buffer, snap-frozen, and stored in 20°C for further Immunoblotting Assay (see below).

HEK293, HEK293T, primary cell culture, and transfections

HEK293 and HEK293T cells were cultured at 95% air and 5% CO_2 in Dulbecco's modified Eagle's medium (Gibco) supplemented with 10% fetal bovine serum (Gibco) and penicillin–streptomycin (Thermo Fisher). Transfections were carried by Lipofectamine 2000 according to the manufacturer's protocol. Lysis was performed in RIPA lysis buffer (150 mM sodium chloride, Triton X-100, 0.5% sodium deoxycholate, 0.1% SDS (sodium dodecyl sulfate), 50 mM Tris, pH 8.0) or NP40 lysis buffer [150 mM sodium chloride 1.0% NP-40, 0.5% sodium deoxycholate, 0.1% SDS (sodium dodecyl sulfate), 50 mM Tris, pH 8.0 supplemented with 1× protease and phosphatase inhibitor 2, 3 mixture (Sigma)]. Cell lysates were then centrifuged at 15,000 *g* for 20 min, and the supernatant was collected as soluble fraction. Pellet was washed twice with lysis buffer and then resuspended with 500 μl of lysis buffer supplemented with 2% SDS. Pellet was sonicated for 9 s with 3 s on and 3 s off at 60% amplitude. Protein concentration was measured using BCA system, and about 20–60 μg of protein is processed for WB or filter retardation assay.

Primary neuronal cell culture and protein expression and siRNA treatment inhibitor treatment

Primary cultures of Striatal neurons were prepared under the local experimental license (VD2137 and VD3392). Briefly, P0 rat pups were dissected and striatal cells were isolated and dissociated by

repeated pipetting. Cells were pelleted by centrifugation, resuspended in the culture medium [Neurobasal medium (Invitrogen) complemented with 1% B27 (Invitrogen), Pen-Strep, L-Glutamine, and KCl], plated in poly-L-lysine-coated multi-well culture dishes at a density of 150,000 cells/cm^2, and cultured at 37°C in 5% CO_2/air atmosphere. Half the medium was replaced on DIV 4, and half of the medium was replaced weekly thereafter. For lentiviral-mediated protein expression, cultures were infected on day *in vitro* (DIV) 7. Plasmid transfections were carried by Lipofectamine 2000 according to the manufacturer's protocol. The siRNA transfections were carried by Lipofectamine 2000 according to the manufacturer's protocol.

Immunoblotting assay and filter retardation assay

Cells were washed twice with PBS and harvested in either RIPA buffer (20 mM Tris–HCl (pH 8), 150 mM NaCl, 1 mM Na_2 EDTA, 1 mM EGTA, 1% Triton X-100, 1% sodium deoxycholate with protease (Sigma) and phosphatase inhibitors (cocktail 2 and 3) (Sigma)) or NP40 lysis buffer [20 mM Tris–HCl (pH 8), 150 mM NaCl, 1 mM EDTA, 1 mM EGTA, 1% NP40, 1% sodium deoxycholate with protease (Sigma) and phosphatase inhibitors (cocktail 2 and 3) (Sigma)]. Lysates were incubated on ice for 30 min and vortexed every 10 min. Protein extracts were cleared of cell debris by centrifugation at 20,000 *g* for 15 min at 4°C. Samples were divided in to two and were either collected as insoluble pellet fraction or spun homogenates. Insoluble pellet fractions were washed with RIPA buffer and sonicated in RIPA supplemented with 2% SDS with settings 40% amplitude for 9 s (3 s on; 3 s off) and collected as detergent-insoluble fraction and used in filter retardation analysis of HTT aggregates. The protein concentration of the fractions was determined using BCA kit (Thermo Fisher). 30 μg of total or spun protein in Laemmli loading buffer was denatured at 85°C for 5 min and separated by sodium dodecyl sulfate–polyacrylamide gel electrophoresis (SDS–PAGE) on a 7–15% polyacrylamide gel. Proteins were subjected to WB using nitrocellulose membranes. After blocking using Odyssey Blocking Buffer (PBS) (P/N: 927-40000) Li-Cor, Lincoln, Nebraska USA, primary antibody (Appendix Table S1) incubation was carried out overnight at 4°C and secondary antibody incubations for 1 h at room temperature. Protein bands were detected using Odyssey® CLx Imaging System, Li-Cor, Lincoln, Nebraska USA. Filter retardation assay of insoluble fractions was carried out as described previously (Sontag *et al*, 2012; Ochaba *et al*, 2018). 30 μg proteins were passed through a 96-well vacuum filtration apparatus (#1706545; Bio-Rad Laboratories) containing a 0.2-μM cellulose acetate membrane filter (catalog #10404180; Whatman) and prewetted in PBS with 2% SDS. After three washing steps with PBS with 2% SDS, the membrane was fixed, blocked, and incubated with antibodies as previously described. Immunodetected proteins were quantified using the ImageJ software.

Immunoprecipitation

Immunoprecipitation was performed using Dynabeads Protein G (catalog #10004D; Thermo Fisher Scientific) following the manufacturer's instructions and using an HTT-specific antibody (D7F7) or ab105119 or anti-GFP antibody. The pulled-down material was analyzed by SDS/PAGE and WB.

Immunocytochemistry

For immunostaining, cells were grown on poly-L-lysine-coated glass coverslips, infected as described above with different expression vectors. Three days post-infection, cells were fixed with 4% paraformaldehyde in PBS (pH 7.4) for 15 min. After fixing, cells were washed three times with ice-cold PBS and blocked with 10% NGS (Invitrogen) in PBS supplemented with 0.1% Triton X-100 (Sigma). Primary antibody was diluted 1:100 in PBS with 5% NGS and 0.1% Triton X-100, and incubated with the cells overnight at 4°C. Cells were washed three times with PBS and incubated at RT with secondary donkey anti-mouse IgG Alexa 568 (Invitrogen, Carlsbad, CA, USA) in PBS with 1% NGS, followed by three washes with PBS. Images were taken using the same inverted confocal laser scanning microscope with polyvinyl alcohol mounting medium with DABCO (Sigma-Aldrich, St. Louis, Missouri, USA) immersion 63 objective as above. Thioflavin S staining was carried out on fixed cells by incubating with 0.05% thioflavin S (Sigma) for 8 min followed by a wash with 80% ethanol for 5 min (three times) each before the antibody incubations.

Cytoplasmic and nuclear fractionation

The fractionation was carried out as described previously (ten Have *et al*, 2012), adapting to the cell density. 48 h post-transfection, HEK293 cells from 10 cm culture dish were washed 3× times with PBS scraped in PBS (2 ml) and cells were pelleted by centrifuging for 4 min at 200 *g*. Cell pellet was resuspended in 1 ml HEPES lysis buffer (HEPES, pH 7.9, 10 mM, $MgCl_2$ 1.5 mM, KCl 10 mM, DTT 0.5 mM supplemented with protease inhibitor cocktail and phosphatase inhibitor cocktail 2 and 3). Resuspended cells were then transferred into a pre-chilled 7 ml Dounce homogenizer, and the cells were sheared using 10 strokes of a tight pestle. Dounced cells were centrifuged for 5 min at 4°C, 200 *g*. The supernatant was retained as cytoplasmic fraction. The nuclear pellet was resuspended in 1 ml of sucrose 1 (0.25 M sucrose, 10 mM $MgCl_2$), cushioned on top of a layer of 1 ml sucrose 2 (0.35 M sucrose, 0.5 mM $MgCl_2$) by slowly pipetting solution sucrose 1 on top of sucrose 2, and centrifuged for 10 min at 4°C, 1,300 *g*, and the pellet was retained as nuclear fraction. Nuclear fraction was resuspended in 500 μl RIPA buffer and sonicated for 9 s (3 s on 3 s off, at 60% amplitude), and samples were collected as nuclear lysate. The cytoplasmic and nuclear fraction protein was estimated by BCA, and the levels of HTT were monitored WB using HTT antibody, β-tubulin, and lamin-B1.

Nuclear condensation cell death assay

The toxicity experiments were performed in primary cortical and primary striatal neurons according to our established protocol (Arbez *et al*, 2017). Nuclei were stained using Hoechst 3342 (Sigma; 0.2 μg/ml in PBS for 5 min). Automated picture acquisition was performed using a Zeiss Axiovert 200 inverted microscope with a 10× objective. Automatic quantification of the nuclear intensity of transfected cells was performed using Velocity imaging software. The cells were considered dead when their nuclear intensity was

higher than the average intensity plus two standard deviations. Each condition was performed in quadruplicate within each experiment, and each experiment was repeated in at least four independent neuronal preparations for each construct studied.

TUNEL assay

DNA fragmentation was detected using the TUNEL method as described previously (Mahul-Mellier *et al*, 2015). Primary neurons were co-transfected for with HTTex1 16Q or 72Q eGFP along with TBK1 or TBK1 KD for the indicated time. Then, the cells were washed three times with PBS to remove unattached recombinant α-syn and fixed in 4% PFA for 15 min at 4°C. Cells were permeabilized in a solution composed of 0.1% Triton X-100 in 0.1% citrate buffer, pH 6.0, and then washed in PBS buffer before incubation with terminal deoxynucleotide transferase (*In situ* Cell Death Detection Kit; Roche) for 1 h at 37 °C in a solution containing TMR red dUTP. Then, neuronal nuclear marker NeuN and TBK1 were stained, and the cells were washed and stained with secondary antibodies, and then, washed 3 times in PBS and mounted using polyvinyl alcohol (PVA) mounting medium (Sigma-Aldrich). The HTT and kinase-co-transfected TUNEL-positive neurons were counted and plotted.

Singulex assay

A total of 50 μl/well of dilution buffer (6% BSA, 0.8% Triton X-100, 750 mM NaCl, and complete protease inhibitor) was added to a 96-well plate (catalog #P-96–450V-C; Axygen). Samples to be tested were diluted in artificial cerebral spinal fluid (0.3 M NaCl; 6 mM KCl; 2.8 mM $CaCl_2$-$2H_2O$; 1.6 mM $MgCl_2$-$6H_20$; 1.6 mM Na_2HPO_4-$7H_2O$; 0.4 mM NaH_2PO_4-H_2O) supplemented with 1% Tween-20 and complete protease inhibitor in a final volume of 150 μl/well. Finally, 100 μl/well of the MW1 antibody coupled with magnetic particles (appropriately diluted in Erenna Assay Buffer, catalog #02–0474-00; Singulex) was added to the assay plate and incubated for 1 h at room temperature under orbital shaking. The beads were then washed with Erenna System Buffer (catalog #02–0111-00; Singulex) and resuspended using 20 μl/well of the specific detection antibody labeled with D2 fluorophore (or Alexa 647 fluorophore) appropriately diluted in Erenna Assay Buffer. The plate was incubated for 1 h at room temperature under shaking. After washing, the beads were resuspended and transferred to a new 96-well plate. A total of 10 μl/well of Erenna Buffer B (catalog #02–0297-00; Singulex) was added to the beads for elution and incubated for 5 min at room temperature under orbital shaking. The eluted complex was magnetically separated from the beads and transferred to a 384-well plate (Nunc catalog #264573; Sigma-Aldrich), where it was neutralized with 10 μl/well of Erenna Buffer D (catalog #02–0368-00; Singulex). Finally, the 384-well plate was heat-sealed and analyzed with the Erenna Immunoassay System.

MS/MS analysis

Huntingtin immunoprecipitated was loaded on to SDS–PAGE. The bands corresponding to HTT were cut, and in-gel digestion was carried out. Briefly, gel bands were washed 2× with 100 μl 50% ACN/100 mM NH_4CO_3 and 1 × 50 μl CAN; 100 μl of 10 mM DTT in 50 mM TEAB was added and incubated for 45 min, at 37°C, and removed DTT; 100 μl of 15 mM IAM solution in 50 mM TEAB was added, incubated for 1 h, RT, in darkness, and removed IAM; 20 μl chymotrypsin (50 ng/μl) was added, incubated for 5 min; and 40 μl TEAB buffer was added to digest overnight. Digested peptides were extracted by 150 μl 0.1% TFA/50% ACN. Samples were dried and dissolved in 20 μl of 2.5% ACN + 0.1% FA. Then, 3 μl sample was injected into nanoUPLC (Waters) and MS measurement was performed by QExactive (Thermo). All raw data were searched against SwissProt via Mascot and search against a database containing HTTex1 sequence via Byonic 3.5 with the consideration of oxidation of methionine, phosphorylation of serine/threonine, and acetylation of protein N-terminal as variable modifications.

Lentiviral vector production

SIN-W-PGK and SIN-W-tetracycline responsive element (TRE) expression vectors were used for the production of lentiviruses in human cells (HEK293T) using a four-plasmid system as described previously (Hottinger *et al*, 2000). Viral pellets were resuspended in phosphate-buffered saline (PBS) with 0.5% bovine serum albumin and stored at 80°C. Before the utilization, viral stocks were diluted with cell culture medium to a concentration of 1,500 ng p24 antigen/ml as measured by ELISA (RETROtek, Gentaur, Kampenhout, Belgium) and applied to the cell cultures at the concentration of 50 ng p24/ml of culture medium for each virus.

Caenorhabditis elegans RNAi treatment and biochemical analysis

Bacterial clones for RNAi (unc-51 and ikke-1) were obtained from the Ahringer RNAi library (https://www.sourcebioscience.com/life-science-research/clones/rnai-resources/c-elegans-rnai-collection-ahringer/). RNAi clones were grown on LB with ampicillin (100 μg/ml) and tetracycline (12.5 μg/ml) o/n and then grown up from a 1/10 dilution in LB with ampicillin (100 μg/ml) for 7 h, which were used to spot medium treatment plates 6 drops each plate, evenly dispersed across the plate. Worm strains are maintained on standard NGM agar plates for multiple generations growing on OP50. Medium NGM treatment agar plates were prepared for all RNAi clones for both Q15 and Q128 worms in duplicate. 24 h post-incubation of the RNAi clones on the NGM treatment plates, 10 L4s of the corresponding strain were placed on RNAi treatment plates. Post-maturation and egg-laying overnight, the L4s were removed ~18 h later. Worms were harvested ~72 h after removal of matured worms and hatching of the laid eggs. Worms were washed off the plate using M9 and centrifuged at a 400 *g* for 1 min to form a live worm pellet. A small portion of worms were used for the isolation of total mRNA using the TRIzol. The isolated mRNA was transcribed, and qPCR was carried out to determine the relative mRNA level using primers of act-1, ikke-1, and unc-51. Other portions of worms were flash-frozen in liquid nitrogen. 200 μl RIPA buffer (20 mM Tris–HCl (pH 8), 150 mM NaCl, 1 mM Na2 EDTA, 1 mM EGTA, 1% Triton X-100, 1% sodium deoxycholate with protease (Sigma) and phosphatase inhibitors (cocktail 2 and 3) (Sigma)) was added to the frozen pellet and allowed the pellet to thaw on regular ice just until melted. Then, the contents of the tube were sonicated with microtip using the settings: 40% amplitude for 30 s (15 s on; 45 s off) (Zanin *et al*, 2011), and then centrifuged at 20,000 *g* for

20 min, and the supernatant was collected as a soluble protein and used for analysis using the SDS–PAGE followed by WB. The pellets were washed with RIPA buffer and sonicated in 200 µl RIPA supplemented with 2% SDS with settings 40% amplitude for 30 s (15 s on; 45 s off) and collected as detergent-insoluble fraction and used in filter retardation analysis of HTT aggregates.

Generation of transgenic TBK1 KD and TBK1 *Caenorhabditis elegans* lines

Caenorhabditis elegans were cultured according to the standard methods (Lee *et al*, 2017). In short, animals were maintained at 20°C or 15°C on NGM agar plates seeded with *Escherichia coli* (OP50). The Punc-54HTT513(Q15)::YFP or Punc-54HTT513(Q128):: YFP was previously published and expresses HTT N513 tagged with YFP transgene in body wall muscle cells (Lee *et al*, 2017). To generate transgenic TBK1 and TBK1 KD animals, 50 ng/µl of DNA encoding Punc-54 TBK1 or Punc-54 TBK1 KD was microinjected along with Punc-54 DS-Red selection marker into the gonads of adult wild-type hermaphrodites to generate multiple (at least 3) independent lines transmitting extrachromosomal arrays.

Caenorhabditis elegans motility assay

Individual lines coexpressing HTT N513 15Q or 128Q with TBK1 or TBK1 KD were examined at day 5 of adulthood. A single L4 worm of each line was grown in NGM agar plate with OP50 bacteria following standard procedures. Three days after pretreatment, 30 L4 worms were picked from each line and placed on fresh NGM agar plates containing 5-FU to avoid progeny development. At 5th day of adulthood, the video was recorded for each individual line and the motility was measured in speed (mm/s) using the wrMTrck plugin using the ImageJ as described previously (Nussbaum-Krammer *et al*, 2015).

Caenorhabditis elegans lifespan assay

Animals were acclimated at 20°C for at least two generations before initiating lifespan analyses. Forty age-matched L4 larvae were placed on NGM plates seeded with *E. coli* (OP50) and cultured at 20°C. During the reproductive time of their life cycle, animals were transferred away from their progeny by daily passaging to freshly seeded plates. Post-reproductive adults were passaged as needed to prevent starvation. Animals were scored as deceased when they no longer moved upon prodding the head several times with a platinum wire as described previously (Lee *et al*, 2017). Animals that crawled off the plate were censored in statistical analyses by adjusting the total population to the number of animals seen on the plate on a given day.

Data availability

The data presented in the manuscript and appendix are deposited in the BioStudies repository under accession number S-BSST413 (www.ebi.ac.uk/biostudies/studies/S-BSST413).

Expanded View for this article is available online.

Acknowledgements
This work was supported by funding from CHDI and EPFL and NINDS (R01 NS086452 and R21 NS083365). We are grateful to Anne-Laure Mahul-Mellier, Galina Limorenko, Johannes Burtscher, Niran Maharjan, Senthil Kumar Thangaraj, and Somanath Jagannath, EPFL, for critical review of the manuscript. We thank Rajasekhar Kolla for preparing the graphical abstract. We are grateful to staff at the Bio-imaging Core Facility (BioP, EPFL) for their technical support. We thank Driss Boudeffa, EPFL, for the production of lentiviral vectors; Jonathan Ricci, EPFL, for assisting *in vitro* kinase validation; and Elena Gasparotto and Lorène Aeschbach, EPFL, for assisting with neuronal cell culture experiments. We thank Naveed Ziari and Kevin S. Hof, EPFL-LISP-IBI-SV, for assisting with experiments in Fig 5B, C, H, I and Appendix Fig S2 and initial help with the setting up of *C. elegans* model. We thank the proteomics core facility at EPFL's School of Life Sciences and Functional Genomics Center Zurich (FGCZ), ETH Zurich, for their support with the mass spectrometry analysis. We are grateful to Prof. Elise A. Kikis, The University of the South, Sewanee, Tennessee, for the kind gift of HD *C. elegans* model and Prof. Shizuo Akira, WPI Immunology Frontier Research Center, Osaka University, Japan, for the kind gift of *Tbk1*$^{-/-}$ mouse model used in this study.

Author contributions
RNH, ACh, and HAL conceived the project; HAL, RNH, and ACh designed the experiments; RNH performed the experiments in Figs 2A, B, G, and H; 3, 4A, C, E; 5–7; EV2, EV3A–F, H, and I; EV4, EV5A–C, E, and F; and Appendix Fig S2A and C performed the experiments in Figs 1A–C and EV1 and EV3G; and Appendix Fig S1; NZ and KH and LM assisted RNH for the experiments in Fig 5B, C, H, I and Appendix Fig S2. LM and JA supervised the experiments in Fig 5B, C, H, I and Appendix Fig S2. PM performed the experiments in Fig 2C–F. ACa and LP designed and supervised the experiments in Fig 2C–F. NA performed the experiment in Fig 4B and D; CAR conceived the experiments by NA. CL performed the experiment in Fig EV5D; GPB conceived the experiments by CL. MKS-B performed TMA, and analyzed and wrote materials and methods for the experiment in Fig EV5G–I; RLMF and MAC supervised the ethical collection, donor interaction, clinical assessment, and processing of the human tissues for Fig EV5G–I. MD established TMA and directs the TMA facility for required for the experiment in Fig EV5G–I; RF co-designed experiments in Fig EV5G–I. RNH, ACh, and HAL analyzed the data; RNH, ACh, and HAL wrote the draft and completed the final manuscript writing with the contributions from all authors.

Conflict of interest
Prof. Hilal A. Lashuel is the founder and CSO of ND BioSciences.

References

Ahmad L, Zhang SY, Casanova JL, Sancho-Shimizu V (2016) Human TBK1: a gatekeeper of neuroinflammation. *Trends Mol Med* 22: 511 – 527

Aiken CT, Steffan JS, Guerrero CM, Khashwji H, Lukacsovich T, Simmons D, Purcell JM, Menhaji K, Zhu YZ, Green K *et al* (2009) Phosphorylation of threonine 3: implications for Huntingtin aggregation and neurotoxicity. *J Biol Chem* 284: 29427 – 29436

Andresen JM, Gayan J, Djousse L, Roberts S, Brocklebank D, Cherny SS, Group US-VCR, Group HMCR, Cardon LR, Gusella JF *et al* (2007) The relationship between CAG repeat length and age of onset differs for Huntington's disease patients with juvenile onset or adult onset. *Ann Hum Genet* 71: 295 – 301

Arbez N, Ratovitski T, Roby E, Chighladze E, Stewart JC, Ren M, Wang X, Lavery DJ, Ross CA (2017) Post-translational modifications clustering within proteolytic domains decrease mutant huntingtin toxicity. *J Biol Chem* 292: 19238 – 19249

Arrasate M, Mitra S, Schweitzer ES, Segal MR, Finkbeiner S (2004) Inclusion body formation reduces levels of mutant huntingtin and the risk of neuronal death. *Nature* 431: 805 – 810

Atwal RS, Xia J, Pinchev D, Taylor J, Epand RM, Truant R (2007) Huntingtin has a membrane association signal that can modulate huntingtin aggregation, nuclear entry and toxicity. *Hum Mol Genet* 16: 2600 – 2615

Atwal RS, Desmond CR, Caron N, Maiuri T, Xia J, Sipione S, Truant R (2011) Kinase inhibitors modulate huntingtin cell localization and toxicity. *Nat Chem Biol* 7: 453 – 460

Benn CL, Landles C, Li H, Strand AD, Woodman B, Sathasivam K, Li SH, Ghazi-Noori S, Hockly E, Faruque SM *et al* (2005) Contribution of nuclear and extranuclear polyQ to neurological phenotypes in mouse models of Huntington's disease. *Hum Mol Genet* 14: 3065 – 3078

Bessa C, Soares J, Raimundo L, Loureiro JB, Gomes C, Reis F, Soares ML, Santos D, Dureja C, Chaudhuri SR *et al* (2018) Discovery of a small-molecule protein kinase Cδ-selective activator with promising application in colon cancer therapy. *Cell Death Dis* 9: 23

Binukumar BK, Pelech SL, Sutter C, Shukla V, Amin ND, Grant P, Bhaskar M, Skuntz S, Steiner J, Pant HC (2016) Profiling of p5, a 24 amino acid inhibitory peptide derived from the CDK5 activator, p35 CDKR1 against 70 protein kinases. *J Alzheimers Dis* 54: 525 – 533

Bowie LE, Maiuri T, Alpaugh M, Gabriel M, Arbez N, Galleguillos D, Hung CLK, Patel S, Xia J, Hertz NT *et al* (2018) N6-Furfuryladenine is protective in Huntington's disease models by signaling huntingtin phosphorylation. *Proc Natl Acad Sci USA* 115: E7081 – E7090

Branco-Santos J, Herrera F, Pocas GM, Pires-Afonso Y, Giorgini F, Domingos PM, Outeiro TF (2017) Protein phosphatase 1 regulates huntingtin exon 1 aggregation and toxicity. *Hum Mol Genet* 26: 3763 – 3775

Bugg CW, Isas JM, Fischer T, Patterson PH, Langen R (2012) Structural features and domain organization of huntingtin fibrils. *J Biol Chem* 287: 31739 – 31746

Bustamante MB, Ansaloni A, Pedersen JF, Azzollini L, Cariulo C, Wang ZM, Petricca L, Verani M, Puglisi F, Park H *et al* (2015) Detection of huntingtin exon 1 phosphorylation by Phos-Tag SDS-PAGE: predominant phosphorylation on threonine 3 and regulation by IKKbeta. *Biochem Biophys Res Comm* 463: 1317 – 1322

Cariulo C, Azzollini L, Verani M, Martufi P, Boggio R, Chiki A, Deguire SM, Cherubini M, Gines S, Marsh JL *et al* (2017) Phosphorylation of huntingtin at residue T3 is decreased in Huntington's disease and modulates mutant huntingtin protein conformation. *Proc Natl Acad Sci USA* 114: E10809 – E10818

Cariulo C, Verani M, Martufi P, Azzollini L, Lavery D, Lee R, Toledo-Sherman L, Doherty E, Lashuel H, Petricca L *et al* (2019) Ultrasensitive, quantitative measurement of huntingtin phosphorylation at residue S13. *Biochem Biophys Res Commun* 521: 549 – 554

Caron NS, Desmond CR, Xia J, Truant R (2013) Polyglutamine domain flexibility mediates the proximity between flanking sequences in huntingtin. *Proc Natl Acad Sci USA* 110: 14610 – 14615

Chiki A, DeGuire SM, Ruggeri FS, Sanfelice D, Ansaloni A, Wang ZM, Cendrowska U, Burai R, Vieweg S, Pastore A *et al* (2017) Mutant Exon1 huntingtin aggregation is regulated by T3 phosphorylation-induced structural changes and crosstalk between T3 phosphorylation and acetylation at K6. *Angew Chem* 56: 5202 – 5207

Cool B, Zinker B, Chiou W, Kifle L, Cao N, Perham M, Dickinson R, Adler A, Gagne G, Iyengar R *et al* (2006) Identification and characterization of a small molecule AMPK activator that treats key components of type 2 diabetes and the metabolic syndrome. *Cell Metab* 3: 403 – 416

Cornett J, Cao F, Wang CE, Ross CA, Bates GP, Li SH, Li XJ (2005) Polyglutamine expansion of huntingtin impairs its nuclear export. *Nat Genet* 37: 198 – 204

Cortes CJ, La Spada AR (2014) The many faces of autophagy dysfunction in Huntington's disease: from mechanism to therapy. *Drug Discov Today* 19: 963 – 971

Cui X, Liang Q, Liang Y, Lu M, Ding Y, Lu B (2014) TR-FRET assays of Huntingtin protein fragments reveal temperature and polyQ length-dependent conformational changes. *Sci Rep* 4: 5601

Cummings BS, Schnellmann RG (2004) Measurement of cell death in mammalian cells. *Curr Protoc Pharmacol* Chapter 12: Unit 12 8

Daldin M, Fodale V, Cariulo C, Azzollini L, Verani M, Martufi P, Spiezia MC, Deguire SM, Cherubini M, Macdonald D *et al* (2017) Polyglutamine expansion affects huntingtin conformation in multiple Huntington's disease models. *Sci Rep* 7: 5070

Deguire SM, Ruggeri FS, Fares MB, Chiki A, Cendrowska U, Dietler G, Lashuel HA (2018) N-terminal Huntingtin (Htt) phosphorylation is a molecular switch regulating Htt aggregation, helical conformation, internalization, and nuclear targeting. *J Biol Chem 293*: 18540 – 18558

Dephoure N, Gould KL, Gygi SP, Kellogg DR (2013) Mapping and analysis of phosphorylation sites: a quick guide for cell biologists. *Mol Biol Cell* 24: 535 – 542

Di Pardo A, Maglione V, Alpaugh M, Horkey M, Atwal RS, Sassone J, Ciammola A, Steffan JS, Fouad K, Truant R *et al* (2012) Ganglioside GM1 induces phosphorylation of mutant huntingtin and restores normal motor behavior in Huntington disease mice. *Proc Natl Acad Sci USA* 109: 3528 – 3533

Ehrlich ME (2012) Huntington's disease and the striatal medium spiny neuron: cell-autonomous and non-cell-autonomous mechanisms of disease. *Neurotherapeutics* 9: 270 – 284

Ehrnhoefer DE, Sutton L, Hayden MR (2011) Small changes, big impact: posttranslational modifications and function of huntingtin in Huntington disease. *Neuroscientist* 17: 475 – 492

Fodale V, Kegulian NC, Verani M, Cariulo C, Azzollini L, Petricca L, Daldin M, Boggio R, Padova A, Kuhn R *et al* (2014) Polyglutamine- and temperature-dependent conformational rigidity in mutant huntingtin revealed by immunoassays and circular dichroism spectroscopy. *PLoS ONE* 9: e112262

Freischmidt A, Wieland T, Richter B, Ruf W, Schaeffer V, Muller K, Marroquin N, Nordin F, Hubers A, Weydt P *et al* (2015) Haploinsufficiency of TBK1 causes familial ALS and fronto-temporal dementia. *Nat Neurosci* 18: 631 – 636

Freischmidt A, Muller K, Ludolph AC, Weishaupt JH, Andersen PM (2017) Association of mutations in TBK1 with sporadic and familial amyotrophic lateral sclerosis and frontotemporal dementia. *JAMA Neurol* 74: 110 – 113

Gu X, Greiner ER, Mishra R, Kodali R, Osmand A, Finkbeiner S, Steffan JS, Thompson LM, Wetzel R, Yang XW (2009) Serines 13 and 16 are critical determinants of full-length human mutant huntingtin induced disease pathogenesis in HD mice. *Neuron* 64: 828 – 840

ten Have S, Hodge K, Lamond AI (2012) *Dynamic proteomics: methodologies and analysis, functional genomics, Germana Meroni and Francesca Petrera*. London: IntechOpen, Available from: https://www.intechopen.com/books/functional-genomics/dynamic-proteomics-methodologies-and-analysis

Havel LS, Wang CE, Wade B, Huang B, Li S, Li XJ (2011) Preferential accumulation of N-terminal mutant huntingtin in the nuclei of striatal

neurons is regulated by phosphorylation. *Hum Mol Genet* 20: 1424 – 1437

Hemmi H, Takeuchi O, Sato S, Yamamoto M, Kaisho T, Sanjo H, Kawai T, Hoshino K, Takeda K, Akira S (2004) The roles of two IkappaB kinase-related kinases in lipopolysaccharide and double stranded RNA signaling and viral infection. *J Exp Med* 199: 1641 – 1650

Hodges A, Strand AD, Aragaki AK, Kuhn A, Sengstag T, Hughes G, Elliston LA, Hartog C, Goldstein DR, Thu D *et al* (2006) Regional and cellular gene expression changes in human Huntington's disease brain. *Hum Mol Genet* 15: 965 – 977

Hottinger AF, Azzouz M, Deglon N, Aebischer P, Zurn AD (2000) Complete and long-term rescue of lesioned adult motoneurons by lentiviral-mediated expression of glial cell line-derived neurotrophic factor in the facial nucleus. *J Neurosci* 20: 5587 – 5593

Kiriyama Y, Nochi H (2015) The function of autophagy in neurodegenerative diseases. *Int J Mol Sci* 16: 26797 – 26812

Klionsky DJ, Abdelmohsen K, Abe A, Abedin MJ, Abeliovich H, Acevedo Arozena A, Adachi H, Adams CM, Adams PD, Adeli K *et al* (2016) Guidelines for the use and interpretation of assays for monitoring autophagy. *Autophagy* 12: 1 – 222

Korac J, Schaeffer V, Kovacevic I, Clement AM, Jungblut B, Behl C, Terzic J, Dikic I (2013) Ubiquitin-independent function of optineurin in autophagic clearance of protein aggregates. *J Cell Sci* 126: 580 – 592

Lee AL, Ung HM, Sands LP, Kikis EA (2017) A new *Caenorhabditis elegans* model of human huntingtin 513 aggregation and toxicity in body wall muscles. *PLoS ONE* 12: e0173644

Lee J-M, Correia K, Loupe J, Kim K-H, Barker D, Hong EP, Chao MJ, Long JD, Lucente D, Vonsattel JPG *et al* (2019) CAG repeat not polyglutamine length determines timing of huntington's disease onset. *Cell* 178: 887 – 900.e14

Lehmann S, Bass JJ, Szewczyk NJ (2013) Knockdown of the *C. elegans* kinome identifies kinases required for normal protein homeostasis, mitochondrial network structure, and sarcomere structure in muscle. *Cell Commun Signal* 11: 71

Lin HK, Boatz JC, Krabbendam IE, Kodali R, Hou Z, Wetzel R, Dolga AM, Poirier MA, van der Wel PCA (2017) Fibril polymorphism affects immobilized non-amyloid flanking domains of huntingtin exon1 rather than its polyglutamine core. *Nat Commun* 8: 15462

Mahul-Mellier AL, Vercruysse F, Maco B, Ait-Bouziad N, De Roo M, Muller D, Lashuel HA (2015) Fibril growth and seeding capacity play key roles in alpha-synuclein-mediated apoptotic cell death. *Cell Death Differ* 22: 2107 – 2122

Maiuri T, Woloshansky T, Xia J, Truant R (2013) The huntingtin N17 domain is a multifunctional CRM1 and Ran-dependent nuclear and cilial export signal. *Hum Mol Genet* 22: 1383 – 1394

Manning G (2005) Genomic overview of protein kinases (December 13, 2005), In *The C. elegans Research Community, WormBook*, WormBook (ed), http://www.wormbook.org

Matsumoto G, Wada K, Okuno M, Kurosawa M, Nukina N (2011) Serine 403 phosphorylation of p62/SQSTM1 regulates selective autophagic clearance of ubiquitinated proteins. *Mol Cell* 44: 279 – 289

Matsumoto G, Shimogori T, Hattori N, Nukina N (2015) TBK1 controls autophagosomal engulfment of polyubiquitinated mitochondria through p62/SQSTM1 phosphorylation. *Hum Mol Genet* 24: 4429 – 4442

McIver EG, Bryans J, Birchall K, Chugh J, Drake T, Lewis SJ, Osborne J, Smiljanic-Hurley E, Tsang W, Kamal A *et al* (2012) Synthesis and structure-activity relationships of a novel series of pyrimidines as potent inhibitors of TBK1/IKKepsilon kinases. *Bioorg Med Chem Lett* 22: 7169 – 7173

Menalled LB, Kudwa AE, Miller S, Fitzpatrick J, Watson-Johnson J, Keating N, Ruiz M, Mushlin R, Alosio W, McConnell K *et al* (2012) Comprehensive behavioral and molecular characterization of a new knock-in mouse model of Huntington's disease: zQ175. *PLoS ONE* 7: e49838

Mende-Mueller LM, Toneff T, Hwang S-R, Chesselet M-F, Hook VYH (2001) Tissue-specific proteolysis of huntingtin (htt) in human brain: evidence of enhanced levels of N- and C-terminal htt fragments in Huntington's disease striatum. *J Neurosci* 21: 1830 – 1837

Menzies FM, Fleming A, Caricasole A, Bento CF, Andrews SP, Ashkenazi A, Fullgrabe J, Jackson A, Jimenez Sanchez M, Karabiyik C *et al* (2017) Autophagy and neurodegeneration: pathogenic mechanisms and therapeutic opportunities. *Neuron* 93: 1015 – 1034

Mishra R, Hoop CL, Kodali R, Sahoo B, van der Wel PC, Wetzel R (2012) Serine phosphorylation suppresses huntingtin amyloid accumulation by altering protein aggregation properties. *J Mol Biol* 424: 1 – 14

Miyasaka T, Ding Z, Gengyo-Ando K, Oue M, Yamaguchi H, Mitani S, Ihara Y (2005) Progressive neurodegeneration in *C. elegans* model of tauopathy. *Neurobiol Dis* 20: 372 – 383

Nixon RA (2013) The role of autophagy in neurodegenerative disease. *Nat Med* 19: 983 – 997

Nussbaum-Krammer CI, Neto MF, Brielmann RM, Pedersen JS, Morimoto RI (2015) Investigating the spreading and toxicity of prion-like proteins using the metazoan model organism *C. elegans*. *J Vis Exp* 52321 . https://doi.org/10.3791/52321

Oakes JA, Davies MC, Collins MO (2017) TBK1: a new player in ALS linking autophagy and neuroinflammation. *Mol Brain* 10: 5

Ochaba J, Lukacsovich T, Csikos G, Zheng S, Margulis J, Salazar L, Mao K, Lau AL, Yeung SY, Humbert S *et al* (2014) Potential function for the Huntingtin protein as a scaffold for selective autophagy. *Proc Natl Acad Sci USA* 111: 16889 – 16894

Ochaba J, Morozko EL, O'Rourke JG, Thompson LM (2018) Fractionation for resolution of soluble and insoluble huntingtin species. *J Vis Exp* 57082 . https://doi.org/10.3791/57082

Ochaba J, Fote G, Kachemov M, Thein S, Yeung SY, Lau AL, Hernandez S, Lim RG, Casale M, Neel MJ *et al* (2019) IKKbeta slows Huntington's disease progression in R6/1 mice. *Proc Natl Acad Sci USA* 116: 10952 – 10961

Oueslati A, Schneider BL, Aebischer P, Lashuel HA (2013) Polo-like kinase 2 regulates selective autophagic alpha-synuclein clearance and suppresses its toxicity *in vivo*. *Proc Natl Acad Sci USA* 110: E3945 – E3954

Paleologou KE, Schmid AW, Rospigliosi CC, Kim HY, Lamberto GR, Fredenburg RA, Lansbury PT Jr, Fernandez CO, Eliezer D, Zweckstetter M *et al* (2008) Phosphorylation at Ser-129 but not the phosphomimics S129E/D inhibits the fibrillation of alpha-synuclein. *J Biol Chem* 283: 16895 – 16905

Perry AK, Chow EK, Goodnough JB, Yeh WC, Cheng G (2004) Differential requirement for TANK-binding kinase-1 in type I interferon responses to toll-like receptor activation and viral infection. *J Exp Med* 199: 1651 – 1658

Pilli M, Arko-Mensah J, Ponpuak M, Roberts E, Master S, Mandell MA, Dupont N, Ornatowski W, Jiang S, Bradfute SB *et al* (2012) TBK-1 promotes autophagy-mediated antimicrobial defense by controlling autophagosome maturation. *Immunity* 37: 223 – 234

Qi L, Zhang XD, Wu JC, Lin F, Wang J, DiFiglia M, Qin ZH (2012) The role of chaperone-mediated autophagy in huntingtin degradation. *PLoS ONE* 7: e46834

Ravikumar B, Duden R, Rubinsztein DC (2002) Aggregate-prone proteins with polyglutamine and polyalanine expansions are degraded by autophagy. *Hum Mol Genet* 11: 1107 – 1117

Ravikumar B, Vacher C, Berger Z, Davies JE, Luo S, Oroz LG, Scaravilli F, Easton DF, Duden R, O'Kane CJ *et al* (2004) Inhibition of mTOR induces

autophagy and reduces toxicity of polyglutamine expansions in fly and mouse models of Huntington disease. *Nat Genet* 36: 585 – 595

Regulier E, Trottier Y, Perrin V, Aebischer P, Deglon N (2003) Early and reversible neuropathology induced by tetracycline-regulated lentiviral overexpression of mutant huntingtin in rat striatum. *Hum Mol Genet* 12: 2827 – 2836

Reif A, Chiki A, Ricci J, Lashuel HA (2018) Generation of native, untagged huntingtin Exon1 monomer and fibrils using a SUMO fusion strategy. *J Vis Exp* 57506 . https://doi.org/10.3791/57506

Richter B, Sliter DA, Herhaus L, Stolz A, Wang C, Beli P, Zaffagnini G, Wild P, Martens S, Wagner SA *et al* (2016) Phosphorylation of OPTN by TBK1 enhances its binding to Ub chains and promotes selective autophagy of damaged mitochondria. *Proc Natl Acad Sci USA* 113: 4039 – 4044

Ritch R, Darbro B, Menon G, Khanna CL, Solivan-Timpe F, Roos BR, Sarfarzi M, Kawase K, Yamamoto T, Robin AL *et al* (2014) TBK1 gene duplication and normal-tension glaucoma. *JAMA Ophthalmol* 132: 544 – 548

Rockabrand E, Slepko N, Pantalone A, Nukala VN, Kazantsev A, Marsh JL, Sullivan PG, Steffan JS, Sensi SL, Thompson LM (2007) The first 17 amino acids of Huntingtin modulate its sub-cellular localization, aggregation and effects on calcium homeostasis. *Hum Mol Genet* 16: 61 – 77

Rose C, Menzies FM, Renna M, Acevedo-Arozena A, Corrochano S, Sadiq O, Brown SD, Rubinsztein DC (2010) Rilmenidine attenuates toxicity of polyglutamine expansions in a mouse model of Huntington's disease. *Hum Mol Genet* 19: 2144 – 2153

Rui Y-N, Xu Z, Patel B, Chen Z, Chen D, Tito A, David G, Sun Y, Stimming EF, Bellen HJ *et al* (2015) Huntingtin functions as a scaffold for selective macroautophagy. *Nat Cell Biol* 17: 262

Saudou F, Humbert S (2016) The biology of huntingtin. *Neuron* 89: 910 – 926

Scherzinger E, Sittler A, Schweiger K, Heiser V, Lurz R, Hasenbank R, Bates GP, Lehrach H, Wanker EE (1999) Self-assembly of polyglutamine-containing huntingtin fragments into amyloid-like fibrils: implications for Huntington's disease pathology. *Proc Natl Acad Sci USA* 96: 4604 – 4609

Scrivo A, Bourdenx M, Pampliega O, Cuervo AM (2018) Selective autophagy as a potential therapeutic target for neurodegenerative disorders. *Lancet Neurol* 17: 802 – 815

Seo H, Sonntag KC, Isacson O (2004) Generalized brain and skin proteasome inhibition in Huntington's disease. *Ann Neurol* 56: 319 – 328

Sontag EM, Lotz GP, Yang G, Sontag CJ, Cummings BJ, Glabe CG, Muchowski PJ, Thompson LM (2012) Detection of mutant huntingtin aggregation conformers and modulation of SDS-soluble fibrillar oligomers by small molecules. *J Huntingtons Dis* 1: 119 – 132

Sorrentino V, Romani M, Mouchiroud L, Beck JS, Zhang H, D'Amico D, Moullan N, Potenza F, Schmid AW, Rietsch S *et al* (2017) Enhancing mitochondrial proteostasis reduces amyloid-beta proteotoxicity. *Nature* 552: 187 – 193

Spilman P, Podlutskaya N, Hart MJ, Debnath J, Gorostiza O, Bredesen D, Richardson A, Strong R, Galvan V (2010) Inhibition of mTOR by rapamycin abolishes cognitive deficits and reduces amyloid-beta levels in a mouse model of Alzheimer's disease. *PLoS ONE* 5: e9979

Steffan JS, Agrawal N, Pallos J, Rockabrand E, Trotman LC, Slepko N, Illes K, Lukacsovich T, Zhu YZ, Cattaneo E *et al* (2004) SUMO modification of Huntingtin and Huntington's disease pathology. *Science* 304: 100 – 104

Szczepanowska J, Ramachandran U, Herring CJ, Gruschus JM, Qin J, Korn ED, Brzeska H (1998) Effect of mutating the regulatory phosphoserine and conserved threonine on the activity of the expressed catalytic domain of Acanthamoeba myosin I heavy chain kinase. *Proc Natl Acad Sci USA* 95: 4146 – 4151

Tanaka M, Machida Y, Niu S, Ikeda T, Jana NR, Doi H, Kurosawa M, Nekooki M, Nukina N (2004) Trehalose alleviates polyglutamine-mediated pathology in a mouse model of Huntington disease. *Nat Med* 10: 148 – 154

Thompson LM, Aiken CT, Kaltenbach LS, Agrawal N, Illes K, Khoshnan A, Martinez-Vincente M, Arrasate M, O'Rourke JG, Khashwji H *et al* (2009) IKK phosphorylates Huntingtin and targets it for degradation by the proteasome and lysosome. *J Cell Biol* 187: 1083 – 1099

Trettel F, Rigamonti D, Hilditch-Maguire P, Wheeler VC, Sharp AH, Persichetti F, Cattaneo E, MacDonald ME (2000) Dominant phenotypes produced by the HD mutation in STHdh(Q111) striatal cells. *Hum Mol Genet* 9: 2799 – 2809

Wang H, Lim PJ, Yin C, Rieckher M, Vogel BE, Monteiro MJ (2006) Suppression of polyglutamine-induced toxicity in cell and animal models of Huntington's disease by ubiquilin. *Hum Mol Genet* 15: 1025 – 1041

Weidberg H, Shvets E, Elazar Z (2011) Biogenesis and cargo selectivity of autophagosomes. *Annu Rev Biochem* 80: 125 – 156

Wexler NS, Lorimer J, Porter J, Gomez F, Moskowitz C, Shackell E, Marder K, Penchaszadeh G, Roberts SA, Gayan J *et al* (2004) Venezuelan kindreds reveal that genetic and environmental factors modulate Huntington's disease age of onset. *Proc Natl Acad Sci USA* 101: 3498 – 3503

Wu Y, Li X, Zhu JX, Xie W, Le W, Fan Z, Jankovic J, Pan T (2011) Resveratrol-activated AMPK/SIRT1/autophagy in cellular models of Parkinson's disease. *Neurosignals* 19: 163 – 174

Yamamoto A, Lucas JJ, Hen R (2000) Reversal of neuropathology and motor dysfunction in a conditional model of Huntington's disease. *Cell* 101: 57 – 66

Zanin E, Dumont J, Gassmann R, Cheeseman I, Maddox P, Bahmanyar S, Carvalho A, Niessen S, Yates JR IIII, Oegema K *et al* (2011) Affinity purification of protein complexes in *C. elegans*. *Methods Cell Biol* 106: 289 – 322

Zheng Z, Li A, Holmes BB, Marasa JC, Diamond MI (2013) An N-terminal nuclear export signal regulates trafficking and aggregation of Huntingtin (Htt) protein exon 1. *J Biol Chem* 288: 6063 – 6071